

# Ultrafast Coulomb-induced dynamics of 2D magnetoexcitons

T. V. Shahbazyan and N. Primožich

*Department of Physics and Astronomy, Vanderbilt University, Nashville, TN 37235*

I. E. Perakis

*Department of Physics and Astronomy, Vanderbilt University, Nashville, TN 37235 and  
Department of Physics, University of Crete, P.O. Box 2208, 710 03, Heraklion, Crete, Greece*

## Abstract

We study theoretically the ultrafast nonlinear optical response of quantum well excitons in a perpendicular magnetic field. We show that for magnetoexcitons confined to the lowest Landau levels, the third-order four-wave-mixing (FWM) polarization is dominated by the exciton-exciton interaction effects. For repulsive interactions, we identify two regimes in the time-evolution of the optical polarization characterized by exponential and *power law* decay of the FWM signal. We describe these regimes by deriving an analytical solution for the memory kernel of the two-exciton wave-function in strong magnetic field. For strong exciton-exciton interactions, the decay of the FWM signal is governed by an antibound resonance with an interaction-dependent decay rate. For weak interactions, the continuum of exciton-exciton scattering states leads to a long tail of the time-integrated FWM signal for negative time delays, which is described by the product of a power law and a logarithmic factor. By combining this analytic solution with numerical calculations, we study the crossover between the exponential and non-exponential regimes as a function of magnetic field. For attractive exciton-exciton interaction, we show that the time-evolution of the FWM signal is dominated by the biexcitonic effects.

arXiv:cond-mat/0008417v1 29 Aug 2000

## I. INTRODUCTION

During recent years, the role of many-body correlations has been a dominant theme in the studies of the ultrafast nonlinear optical response of semiconductors in the coherent regime.<sup>1</sup> In the lowest order in the optical fields, the nonlinear optical polarization comes from the excitation of two electron-hole ( $e$ - $h$ ) pair states. The Coulomb interactions between these elementary excitations govern the spectral and temporal properties of the nonlinear optical response.<sup>2-4</sup>

In noninteracting systems, such as atom-like two-level systems, the only source of optical nonlinearity is the Pauli blocking. This introduces local correlations, due to the phase space filling, between the carriers excited by the pump and the probe optical pulses, which are separated by a time delay  $\tau$ .<sup>5</sup> The Coulomb interaction brings about new nonlinearities by changing the dynamics of the photoexcited  $e$ - $h$  pairs. The simplest theoretical approach that accounts for the interactions between photoexcited  $e$ - $h$  pairs is the time-dependent Hartree-Fock approximation, which leads to the well known semiconductor Bloch equations (SBE).<sup>6-10,2</sup> The latter have been successfully used to describe a variety of experimental results, including, e.g., the ac Stark effect and Rabi oscillations,<sup>7,10,2</sup> the fast exponential decay of the time-integrated (TI) four-wave-mixing (FWM) signal for negative time delays ( $\tau < 0$ ),<sup>11,12</sup> the time-dependence of the time-resolved (TR) FWM signal<sup>11-13</sup>, the photon echoes coming from the continuum of states,<sup>14,15</sup> and some aspects of phase measurements.<sup>16,17</sup> Being a mean-field approach, the SBE's replace the Coulomb interactions by a spatially-averaged effective field of all the photoexcited excitons, and thus neglect correlations due to exciton-exciton scattering and bound biexciton states.

More recent experiments indicated the importance of Coulomb correlations, e.g., in the dependence of the nonlinear response on the polarization of the optical fields.<sup>18,1</sup> Many of the experimental results have been explained in terms of excitation-induced dephasing,<sup>19-22</sup> and exciton-exciton scattering processes.<sup>23-25</sup> The importance of bound biexciton states in FWM was also pointed out, e.g., in Refs. 26-32. Exciton-exciton correlations have been shown to play a significant role in the ac Stark effect<sup>33</sup> and in quantum beats.<sup>34</sup> Several systematic methods for incorporating many-particle correlations in the coherent nonlinear optical response have been developed,<sup>18</sup> including the effective exciton Hamiltonian approach,<sup>35-37,3</sup> the coherently controlled truncation scheme,<sup>38-40,25</sup> the correlation function approach,<sup>42-44</sup> and the canonical transformation approach.<sup>45-51</sup>

In this paper, we study the role of exciton-exciton correlations on the ultrafast nonlinear optical response of quantum well (QW) excitons in a perpendicular magnetic field  $\mathbf{B}$ . The effect of a magnetic field on the photoexcited carriers is twofold. First, the conduction and valence bands collapse into discrete sets of highly degenerate Landau levels (LL). The magnetic field squeezes the electron and hole wave functions (magnetic confinement). The relative importance of the Coulomb versus magnetic confinement in determining the exciton states depends on the ratio  $\omega_c/2E_B = (a_B/l)^2$ , where  $a_B$  and  $E_B$  are the exciton Bohr radius and binding energy at zero field, while  $l = \sqrt{1/eB}$  and  $\omega_c$  are the magnetic length and the cyclotron frequency, respectively (we set  $\hbar = 1$ ). With increasing magnetic field, the crossover from Coulomb-bound excitons to magnetoexcitons occurs for  $l \lesssim a_B$ , where the binding energy of the 2D magnetoexciton,  $E_0 \sim e^2/l$ , exceeds the Bohr energy  $E_B \sim e^2/a_B$ . In typical GaAs/AlGaAs quantum wells, this crossover to the strong magnetic field regime

occurs for  $B \gtrsim 4$  T.

The second effect of the magnetic field is that, by freezing the kinetic energy of the photoexcited carriers in two spatial dimensions, it increases the relative strength of the exciton-exciton interactions.<sup>52–65</sup> In bulk semiconductors, FWM experiments showed a strong enhancement of the FWM signal with increasing magnetic field.<sup>61–63</sup> At the same time, the time-integrated signal exhibited a long non-Markovian decay for negative time delays.<sup>61–63</sup>

In QW's, the exciton-exciton interactions are expected to dominate the coherent optical dynamics as the magnetic field increases. When the LL separation exceeds the magnetoexciton binding energy,  $\omega_c/|E_0| \sim a_B/l \gg 1$ , the inter-LL transitions are suppressed and the optical response is determined by magnetoexcitons confined to the lowest LL (LLL). Note that, in an ideal 2D system, the interactions between magnetoexcitons with zero center of mass momentum are suppressed due to the electron-hole symmetry.<sup>66–68</sup> In realistic QW's, however, this symmetry is lifted due to, e.g., the differing band offsets, lateral confinement, and disorder.<sup>69</sup> As was first pointed out in Refs. 64,65, the  $e$ - $h$  asymmetry plays an important role in the nonlinear response of magnetoexcitons in QW's.

We investigate here the role of four-particle correlations in the coherent ultrafast dynamics of 2D magnetoexcitons confined to the LLL. Using the canonical transformation formalism<sup>46,47,49</sup>, we show that, due to the discrete nature of LL's, the third-order FWM polarization is determined by a momentum-independent two-exciton amplitude  $\chi(t)$ , satisfying a simple equation

$$i\partial_t\chi(t) - 2\Omega_0\chi(t) = V^{HF}p^2(t) + F(t), \quad (1)$$

where  $\Omega_0$  is the pump detuning from the magnetoexciton level. The first source term in the rhs represent the two pump-induced polarizations,  $p(t)$ , interacting via the Hartree-Fock potential  $V^{HF}$ , while  $F(t)$  originates from the exciton-exciton correlations.

We have calculated  $F(t)$  numerically and showed that, for a wide range of parameters, the results can be described in terms of an analytical solution derived for strong magnetic field. In particular,  $\chi(t)$  can be expressed in terms of the Hartree-Fock solution  $\chi^{HF}(t)$  [obtained by setting  $F(t) = 0$  in Eq. (1)] as follows:

$$\chi(t) = \int_{-\infty}^{\infty} dt' S(t-t')\chi^{HF}(t'), \quad (2)$$

where  $S(t)$  represents a *memory kernel* whose time dependence is governed by the exciton-exciton correlations. For sufficiently strong magnetic fields, such that the magnetic length  $l$ , is smaller than the characteristic range of the exciton-exciton potential,  $a$ , we have derived a simple analytic expression for the memory function  $S(\omega)$  in the frequency domain, that incorporates both the biexcitonic and the exciton-exciton scattering effects nonperturbatively.

For attractive exciton-exciton interaction, the biexciton effects dominate. For  $l \ll a$ , when the momentum exchange between excitons is suppressed, we recover the average polarization model (APM).<sup>12,70,25,1,63</sup> For weaker fields, we show that the time-evolution of the FWM signal is determined by both biexcitonic and exciton-exciton scattering effects. For short pump durations, we reproduce the biexciton oscillations in the TI-FWM signal.<sup>65</sup> As the pump duration becomes longer than the biexciton binding energy, we find a crossover between two exponential regimes in the SR- and TI-FWM spectra, originating from different dephasing rates of the exciton and biexciton bound states.

For repulsive exciton-exciton interactions, we find two regimes in the time dependence of the FWM signal governed by a dimensionless parameter  $G \sim u_0 a^2 / E_0 l^2$ , where  $E_0$  is the magnetoexciton binding energy and  $u_0$  is the characteristic strength of the exciton-exciton interactions ( $u_0 < 0$  for repulsive interactions). For  $|G| \gg 1$ , the memory function is dominated by an antibound resonance, made up from the continuum of the exciton-exciton states, with the width  $\gamma_{sc} \sim u_0 G e^{-|G|}$ . In this regime, the TI-FWM signal exhibits oscillations with a period determined by the energy of an antibound state, together with an overall exponential decay characterized by the *interaction-induced* time  $\gamma_{sc}^{-1}$ . For  $|G| \ll 1$ , the long-time behavior of the FWM signal is determined by the singular (logarithmic) low-frequency behavior of  $S(\omega)$ ; this leads to a *power law* decay of the TI-FWM signal for negative time delays: TI-FWM  $\propto \tau^{-2}$  (up to log factor). In the intermediate case  $|G| \sim 1$ , the crossover between the two regime as a function of time delay occurs on the scale  $|\tau| \sim |u_0|^{-1}$ . By combining our analytic solution with numerical calculations, we study the crossover between exponential and non-exponential regimes as a function of magnetic field. Our results demonstrate that four-particle Coulomb correlations lead to a qualitatively different dynamics of the two-exciton excitations as compared to the one-exciton states.

The paper is organized as follows. In Section II, we summarize relevant facts regarding 2D excitons in a strong magnetic field. In Section III we present an expression for the FWM polarization obtained in Appendices A and B. In Section IV, we derive an analytical solution for the two-exciton amplitude in the case of strong magnetic field and in Section V we analyze the memory function in all the regimes of interest. In Section VI, we presents the results of numerical calculations for the FWM polarization and compare them with our analytical solution. Section VII concludes the paper.

## II. 2D EXCITONS IN STRONG MAGNETIC FIELD

In this section, we summarize some basic facts regarding 2D magnetoexcitons.<sup>66–68</sup> We consider the case when the magnetic field is sufficiently strong and the central optical frequency is tuned to transitions between the lowest Landau levels of the conduction and valence bands. In this case, the inter-LL transitions are suppressed so that the photoexcited  $e$ - $h$  pairs are restricted to the LLL. In the Landau gauge,  $\mathbf{A} = (0, Bx)$ , the electron and hole wave-functions,  $\psi_k$  and  $\bar{\psi}_k$ , are characterized by the  $y$ -component of the momentum,  $k = -x_0/l^2$ , where  $x_0$  is the  $x$ -coordinate of the cyclotron orbit center,

$$\psi_k(\mathbf{r}) = \frac{1}{\sqrt{L\pi^{1/2}l}} e^{iky - (x+kl^2)^2/2l^2}, \quad \bar{\psi}_k(\mathbf{r}) = \psi_{-k}^*(\mathbf{r}), \quad (3)$$

( $L$  is the system size). The normalized one-exciton wave function, with total momentum  $\mathbf{p}$ , can be expressed in terms of the electron and hole wave functions as<sup>66–68</sup>

$$\Psi_{\mathbf{p}}(\mathbf{r}_1, \mathbf{r}_2) = N^{-1/2} \sum_k e^{-ikp_x l^2} \psi_{p_y/2+k}(\mathbf{r}_1) \bar{\psi}_{p_y/2-k}(\mathbf{r}_2) = \frac{N^{-1/2}}{2\pi l^2} e^{i\mathbf{p}\cdot\mathbf{R} - iXy/l^2 - (\mathbf{r}+l^2\mathbf{p}\times\mathbf{z})^2/4l^2}, \quad (4)$$

where  $\mathbf{r} = \mathbf{r}_1 - \mathbf{r}_2$ ,  $\mathbf{R} = (\mathbf{r}_1 + \mathbf{r}_2)/2$  are the relative and the average coordinates, respectively,  $N = L^2/2\pi l^2$  is the LL degeneracy, and  $\mathbf{z}$  is the unit vector in the direction of the magnetic

field. The magnetoexciton creation operator is given in terms of the electron and hole operators  $a_k^\dagger$  and  $b_k^\dagger$ , by the similar expression,

$$d_{\mathbf{p}}^\dagger = N^{-1/2} \sum_k e^{-ikp_x l^2} a_{p_y/2+k}^\dagger b_{p_y/2-k}^\dagger. \quad (5)$$

Consider first the spectrum of a single magnetoexciton. In the one-exciton basis, the Hamiltonian  $H_{eh}^{(1)}$  that describes the interaction between an electron and a hole, is diagonal:

$$H_{eh}^{(1)} = \sum_{\mathbf{p}} \varepsilon_p d_{\mathbf{p}}^\dagger d_{\mathbf{p}}, \quad (6)$$

where  $\varepsilon_p$  is the 2D magnetoexciton energy, given by

$$\varepsilon_p = - \int \frac{d\mathbf{q}}{(2\pi)^2} v_q e^{-q^2 l^2 / 2 + i(\mathbf{q} \times \mathbf{p}) \cdot \mathbf{z} l^2} = - \frac{e^2}{\kappa l} \sqrt{\frac{\pi}{2}} e^{-p^2 l^2 / 4} I_0(p^2 l^2 / 4). \quad (7)$$

Here  $v_q = 2\pi e^2 / \kappa q$  is the 2D Coulomb potential ( $\kappa$  is the dielectric constant) and  $I_0(x)$  is the Bessel function. For small center of mass momenta,  $pl \ll 1$ , the magnetoexciton spectrum is parabolic,

$$\varepsilon_p = -E_0 + \frac{p^2}{2M}, \quad M = \frac{8}{3} \sqrt{\frac{2}{\pi}} \frac{\kappa}{e^2 l}, \quad (8)$$

where  $E_0 = \frac{e^2}{\kappa l} \sqrt{\frac{\pi}{2}}$  is the magnetoexciton binding energy and  $M$  is the magnetoexciton effective mass. For large momenta,  $pl \gg 1$ , Eq. (7) yields  $\varepsilon_p = -e^2 / \kappa pl^2$ . Since for strong magnetic field the exciton momentum is proportional to the  $e$ - $h$  separation,  $p \sim r / l^2$ , for large momenta we recover the Coulomb potential between a well-separated electron and hole,  $-e^2 / \kappa r$ . On the other hand, for small momenta, the electron and hole sit on top of each other forming a neutral magnetoexciton with the effective mass  $M$ .<sup>66-68</sup> The one-exciton Hamiltonian is  $H_X = H_0 + H_{eh}^{(1)}$ , where  $H_0$  describes a noninteracting  $e$ - $h$  pair with energy  $E_0^e + E_0^h + E_g - \omega_0 = \bar{E}_g - \omega_0$ , where  $E_0^e$  and  $E_0^h$  are the electron and hole LLL energies, respectively,  $E_g$  is the semiconductor bandgap, and  $\omega_0$  is the pump central frequency (we are working in the rotating frame). The eigenstates of  $H_X$ ,  $|\mathbf{p}\rangle = d_{\mathbf{p}}^\dagger |0\rangle$ , satisfy the eigenvalue equation

$$H_X |\mathbf{p}\rangle = \Omega_p |\mathbf{p}\rangle, \quad \Omega_p = \bar{E}_g + \varepsilon_p - \omega_0. \quad (9)$$

Note that the *linear* response in strong field is similar to that of a two-level system. This can be seen, e.g., by noticing that the optical transition operator,  $U^\dagger$  is proportional to the exciton creation operator [setting  $\mathbf{p}=0$  in Eq. (5)],

$$U^\dagger \equiv \sum_k a_k^\dagger b_{-k}^\dagger = N^{1/2} d_0, \quad (10)$$

so that  $HU^\dagger|0\rangle = N^{1/2} H_X d_0^\dagger |0\rangle = \Omega_0 U^\dagger |0\rangle$ , where  $\Omega_0$  is the detuning from the magnetoexciton level. On the other hand, as we will see later, the *nonlinear* optical response is dominated by the exciton-exciton interactions.

Let us now turn to the two-exciton states which govern the FWM signal. Only states with zero total momentum contribute to the optical response. The normalized two-exciton basis with zero total momentum can be chosen as

$$\Psi_{\mathbf{p}}^{(2)}(\mathbf{r}_1, \mathbf{r}_2; \mathbf{r}'_1, \mathbf{r}'_2) = \Psi_{\mathbf{p}}(\mathbf{r}_1, \mathbf{r}_2)\Psi_{-\mathbf{p}}(\mathbf{r}'_1, \mathbf{r}'_2). \quad (11)$$

Correspondingly, the states  $|\mathbf{p}, -\mathbf{p}\rangle = d_{\mathbf{p}}^\dagger|0\rangle \times d_{-\mathbf{p}}^\dagger|0\rangle$  form a complete basis set of the zero-momentum two-exciton Hilbert subspace. Using Eq. (5), one can easily expand any two-exciton state in this basis. For example,

$$d_0^\dagger d_0^\dagger|0\rangle = d_0^\dagger|0\rangle \times d_0^\dagger|0\rangle - \frac{1}{N} \sum_{\mathbf{p}} d_{\mathbf{p}}^\dagger|0\rangle \times d_{-\mathbf{p}}^\dagger|0\rangle. \quad (12)$$

The matrix elements of the Coulomb potential between four photoexcited particles, two electrons and two holes, evaluated in the two-exciton basis (11), have the form

$$V_{ee}(\mathbf{p}, \mathbf{q}) = v_{|\mathbf{p}-\mathbf{q}|} e^{-(\mathbf{p}-\mathbf{q})^2 l^2/2 - i(\mathbf{p} \times \mathbf{q}) \cdot \mathbf{z} l^2}, \quad (13)$$

$$V_{hh}(\mathbf{p}, \mathbf{q}) = v_{|\mathbf{p}-\mathbf{q}|} e^{-(\mathbf{p}-\mathbf{q})^2 l^2/2 + i(\mathbf{p} \times \mathbf{q}) \cdot \mathbf{z} l^2}, \quad (14)$$

$$V_{eh}(\mathbf{p}, \mathbf{q}) = -2v_{|\mathbf{p}-\mathbf{q}|} e^{-(\mathbf{p}-\mathbf{q})^2 l^2/2} + 2\varepsilon_p \delta_{\mathbf{p}\mathbf{q}}, \quad (15)$$

with  $\varepsilon_p$  given by Eq. (7). The two-exciton matrix elements of the Hamiltonian  $H$  are then given by

$$H(\mathbf{p}, \mathbf{q}) = 2\Omega_p \delta_{\mathbf{p}\mathbf{q}} - V(\mathbf{p}, \mathbf{q})/L^2. \quad (16)$$

The first term is simply the energy of two non-interacting excitons (in the rotating frame). The second term represents the exciton-exciton interaction potential

$$V(\mathbf{p}, \mathbf{q}) = 4v_{|\mathbf{p}-\mathbf{q}|} \sin^2[(\mathbf{p} \times \mathbf{q}) \cdot \mathbf{z} l^2/2] e^{-(\mathbf{p}-\mathbf{q})^2 l^2/2} + V_A(\mathbf{p}, \mathbf{q}) = V_S(\mathbf{p}, \mathbf{q}) + V_A(\mathbf{p}, \mathbf{q}). \quad (17)$$

The potential  $V_A(\mathbf{p}, \mathbf{q})$  describes the contribution to the exciton-exciton interactions in the quasi-2D case that comes from the lifting of the electron-hole symmetry in a strong magnetic field by, e.g., the differing band offsets, the lateral confinement, and the disorder.<sup>67,64</sup> Such an asymmetry can be strong in typical quantum wells and plays an important role in the nonlinear optical response in QW's.<sup>64,69</sup>

Note here that the symmetric part of the exciton-exciton potential,  $V_S(\mathbf{p}, \mathbf{q})$ , and the exciton dispersion are not independent, but are related as follows:

$$2\varepsilon_p - 2\varepsilon_0 = \int \frac{d\mathbf{q}}{(2\pi)^2} V_S(\mathbf{p}, \mathbf{q}). \quad (18)$$

This relation reflects the two possible ways of arranging two electrons and two holes into two excitons.

Note also that  $V_S(\mathbf{p}, \mathbf{q})$  vanishes for zero momenta. This reflects the fact that, due to the electron and hole symmetry in the ideal 2D case, the net interaction between two magnetoexcitons vanishes at small  $e$ - $h$  separation (which corresponds to small momenta). In contrast, the potential  $V_A(\mathbf{p}, \mathbf{q})$ , originating from the breaking of the  $e$ - $h$  symmetry in a QW,<sup>69</sup> is finite for small momenta and leads to the main interaction-induced contribution to the FWM signal.<sup>64,65</sup>

### III. THIRD-ORDER OPTICAL RESPONSE OF 2D MAGNETOEXCITONS

As discussed in the Introduction, the calculation of the magnetoexciton nonlinear optical response in QW's is simplified considerably due to the "freezing" of the kinetic energy of electrons and holes by strong perpendicular magnetic field. Using the canonical transformation method,<sup>46,47</sup> outlined in Appendix A, we have obtained a simple expression for the FWM polarization  $\tilde{P}_{XX}$  that comes from the exciton-exciton interactions. Referring the reader to Appendix B for the derivation, the result reads

$$\tilde{P}_{XX}(t, \tau) = i\mu^2 \mathcal{E}_1 \theta(t + \tau) e^{-\Gamma(t+\tau) - i\omega_0(t-\tau)} \left[ e^{-i\Omega_0(t+\tau)} \chi(-\tau) - e^{i\Omega_0(t+\tau)} \chi(t) \right], \quad (19)$$

Here,  $\mathcal{E}_i(t)$  is the electric field of the probe ( $i = 1$ ) or pump ( $i = 2$ ),  $\mu$  is the interband dipole matrix element,  $\omega_0$  is the central optical frequency,  $\Omega_0$  is the pump detuning from the magnetoexciton level,  $\Gamma$  is the magnetoexciton dephasing rate, and  $\theta(t)$  is the step-function. Since the FWM polarization along the direction  $2\mathbf{k}_2 - \mathbf{k}_1$  is linear in the probe optical field, we assume, for simplicity, a delta-function probe pulse  $\mathcal{E}_1(t) = e^{-i\omega_0\tau} \mathcal{E}_1 \delta(t + \tau)$  and a pump pulse of finite duration  $t_0$  centered at  $t = 0$ .

As can be seen from Eq. (19), the interaction-induced FWM polarization is directly proportional to the two-exciton amplitude  $\chi(t)$ . In Appendix B we show that, in the case of magnetoexcitons in the LLL,  $\chi(t)$  satisfies a simple equation:

$$i\partial_t \chi(t) - 2\Omega_0 \chi(t) = V^{HF} p^2(t) + F(t), \quad (20)$$

where  $p(t)$  is the linear pump polarization, determined by Eq. (B19), and  $V^{HF}$  is the Hartree-Fock interaction given by Eq. (B25). The last term in Eq. (20) describes the effect of four-particle correlations and has the form (see Appendix B)

$$F(t) = \frac{l^2}{\pi} \int d\mathbf{q} V_q^{HF} w_q(t), \quad (21)$$

where  $w_p(t)$  are the coefficients of the expansion of the two-exciton wave-function in the basis (11). As shown in Appendix B, they satisfy the Wannier-like equation

$$i\partial_t w_p(t) - 2\Omega_p w_p(t) = - \int \frac{d\mathbf{q}}{(2\pi)^2} V(\mathbf{p}, \mathbf{q}) w_q(t) + V_p^{HF} p^2(t), \quad (22)$$

where  $V_p^{HF}$  is the Hartree-Fock potential whose explicit expression is given by Eq. (B22). The amplitude  $\chi(t)$  is related to  $w_p(t)$  simply as  $\chi(t) = w_0(t) - N^{-1} \sum_{\mathbf{p}} w_p(t)$  (see Appendix B). The source (last) term in the rhs of Eq. (22) describes the interaction of two pump-induced polarizations,  $p^2(t)$ , via the Hartree-Fock potential  $V_p^{HF}$ , while the first term describes the effect of the exciton-exciton correlations.

The Hartree-Fock approximation corresponds to setting  $F(t) = 0$  in Eq. (20), which yields

$$\chi^{HF}(t) = -iV^{HF} \int_{-\infty}^t dt' e^{-2i\Omega_0(t-t')} p^2(t'), \quad (23)$$

with the pump polarization  $p(t)$  given by the solution of Eq. (B19),

$$p(t) = -i\mu \int_{-\infty}^t dt' e^{-i(\Omega_0 - i\Gamma)(t-t')} \mathcal{E}_2(t'). \quad (24)$$

The FWM polarization within the Hartree-Fock approximation is then obtained by substituting  $\chi^{HF}(t)$  into Eq. (19). The relation between the above formalism and that of Refs. 1,63,25 is discussed in Appendix D.

#### IV. ANALYTIC SOLUTION IN STRONG MAGNETIC FIELD

The role of the exciton-exciton correlations in the FWM polarization is described by the function  $F(t)$ , given by Eq. (21). In order to obtain  $F(t)$ , it is necessary to find the two-exciton amplitude  $w_p(t)$  by solving Eq. (22). In the general case, this can only be done numerically, and the corresponding results are presented in the next section. In this section, we derive an analytical expression for  $w_p(t)$  in the case of strong magnetic field.

As discussed above, the interactions between QW magnetoexcitons, confined to the LLL, contribute to the nonlinear optical polarization only in the presence of electron-hole asymmetry.<sup>64,65</sup> The corresponding potential  $V_A(\mathbf{p}, \mathbf{q})$  is short-ranged, and its specific form depends on the sample.<sup>64</sup> In order to proceed further, we assume the following form for the s-wave component of this potential:

$$V_A(\mathbf{p}, \mathbf{q}) = V_A e^{-(p^2+q^2)a^2/2}, \quad (25)$$

where  $a$  is the potential range. The potential strength is characterized by the energy scale

$$u_0 = \frac{V_A}{4\pi a^2}. \quad (26)$$

With such  $V_A(\mathbf{p}, \mathbf{q})$ , the Hartree-Fock parameters, determined by Eqs. (B22) and (B25), have a simple form,

$$V_p^{HF} = u_0 \left(1 - \frac{a^2}{l^2}\right) e^{-p^2 a^2/2}. \quad (27)$$

and

$$V^{HF} = -u_0 \left(\frac{l}{a} - \frac{a}{l}\right)^2. \quad (28)$$

Turning to Eq. (22), We observe that a considerable simplification occurs for sufficiently strong magnetic field such that  $l < a$ . In this case, the characteristic momenta of the excitons scattered by the potential (25) are small:  $p \sim a^{-1} < l^{-1}$ . Since for small momenta the magnetoexciton size is also small (see Section II), the *symmetric* part of the exciton-exciton potential,  $V_S(\mathbf{p}, \mathbf{q})$ , is suppressed. Indeed, for the characteristic momenta  $p, q \sim 1/a$ , we get from Eq. (17) that  $V_S(\mathbf{p}, \mathbf{q}) \sim e^2 a (l/a)^4$ . Therefore,  $V_S(\mathbf{p}, \mathbf{q})$  can be neglected, as compared to  $V_A(\mathbf{p}, \mathbf{q})$ , under the condition

$$u_0 > E_0 \left(\frac{l}{a}\right)^5, \quad (29)$$



where  $E_0 \sim e^2/\kappa l$  is the magnetoexciton binding energy [see Eq. (8)]. Note that the above condition can be met even for weak asymmetry,  $u_0 \ll E_0$ , provided that the magnetic field is sufficiently strong. Thus, for  $l < a$ , we can replace  $V(\mathbf{p}, \mathbf{q})$  by  $V_A(\mathbf{p}, \mathbf{q})$  in the first term in the rhs of Eq. (22). Then, by using Eqs. (21), (25), and (27), this term can be expressed via  $F(t)$  as

$$-\int \frac{d\mathbf{q}}{(2\pi)^2} V_A(\mathbf{p}, \mathbf{q}) w_q(t) = -\frac{l^2 e^{-p^2 a^2/2}}{\pi(l^2/a^2 - 1)} \int d\mathbf{q} V_q^{HF} w_q(t) = -F(t) \frac{e^{-p^2 a^2/2}}{l^2/a^2 - 1}. \quad (30)$$

Eq. (22) can be solved by Fourier transform:

$$w_p(\omega) = -\frac{e^{-p^2 a^2/2}}{l^2/a^2 - 1} \frac{F(\omega)}{\omega - 2\Omega_p} + \frac{V_p^{HF} p^{(2)}(\omega)}{\omega - 2\Omega_p}, \quad (31)$$

where  $p^{(2)}(\omega)$  is the Fourier transform of  $p^2(t)$ . To find  $F(\omega)$ , we multiply the above equation by  $V_p^{HF}$  and take the sum over  $\mathbf{p}$ . This gives

$$F(\omega) = -\frac{l^2}{\pi} \frac{F(\omega)}{l^2/a^2 - 1} \int d\mathbf{p} \frac{e^{-p^2 a^2/2} V_p^{HF}}{\omega - 2\Omega_p} + p^{(2)}(\omega) \frac{l^2}{\pi} \int d\mathbf{p} \frac{(V_p^{HF})^2}{\omega - 2\Omega_p}, \quad (32)$$

yielding

$$F(\omega) = -V^{HF} p^{(2)}(\omega) \frac{Q(\omega)}{1 + Q(\omega)}, \quad (33)$$

where

$$Q(\omega) = \frac{V_A}{(2\pi)^2} \int d\mathbf{p} \frac{e^{-p^2 a^2}}{\omega - 2\Omega_p}. \quad (34)$$

Using Eq. (33), the amplitude  $\chi(\omega)$  can then be easily obtained from Eq. (20) as

$$\chi(\omega) = \frac{V^{HF} p^{(2)}(\omega)}{\omega - 2\Omega_0} S(\omega), \quad (35)$$

where

$$S(\omega) = \frac{1}{1 + Q(\omega)}. \quad (36)$$

Equations (34-36), which are the main result of this section, provide an analytic expression for the two-exciton amplitude  $\chi(t)$ , which determines the FWM polarization (19). The result (35) has the form of a product of the Hartree-Fock result, Eq. (23), and the *frequency-dependent* factor  $S(\omega)$ :  $\chi(\omega) = \chi^{HF}(\omega) S(\omega)$ . In the time domain,  $\chi(t)$  has the simple form

$$\chi(t) = \int_{-\infty}^{\infty} dt' S(t - t') \chi^{HF}(t') \quad (37)$$

with  $\chi^{HF}(t)$  given by Eq. (23). As can be seen,  $S(t)$  represents a *memory kernel* whose time dependence is governed by the exciton-exciton correlations. In the absence of correlations, corresponding to  $Q(\omega) = 0$  in Eq. (36), the kernel is instantaneous,  $S(t) = \delta(t)$ , and we recover the Hartree-Fock result.

## V. MEMORY FUNCTION

In this Section we analyze the properties of the memory function  $S(\omega)$ , given by Eq. (36). For sufficiently strong magnetic fields such that  $l < a$ , the main contribution to the integral in Eq. (34) comes from small momenta  $q \sim a^{-1} < l^{-1}$ . For such momenta, the exciton dispersion is quadratic,  $\Omega_q \simeq \Omega_0 + q^2/2M$ , where  $M$  is magnetoexciton effective mass [see Eq. (8)]. We then get from Eq. (34)

$$Q(\omega) = V_A \mathcal{N} \int_0^\infty dE \frac{e^{-E/D}}{\omega - 2\Omega_0 - 2E}, \quad (38)$$

where  $\mathcal{N} = M/2\pi = \frac{4}{3\pi}(E_0 l^2)^{-1}$  is the 2D *magnetoexciton* density of states and

$$D = \frac{1}{2Ma^2} = \frac{3E_0}{16} \left(\frac{l}{a}\right)^2 \quad (39)$$

plays the role of the cutoff energy.

For large frequencies,  $|\omega - 2\Omega_0| \gg D$ , the integrand in Eq. (38) can be expanded in terms of  $(\omega - 2\Omega_0)^{-1}$  yielding

$$Q(\omega) \simeq \frac{u_0}{\omega - 2\Omega_0}. \quad (40)$$

For small frequencies,  $|\omega - 2\Omega_0| \ll D$ , the integral in Eq. (38) diverges at the lower limit and can be estimated as

$$Q(\omega) \simeq -G \ln \left| \frac{2D}{\omega - 2\Omega_0} \right| - i\pi G \theta(\omega - 2\Omega_0), \quad (41)$$

where

$$G = \frac{V_A \mathcal{N}}{2} = \frac{8}{3} \frac{u_0}{E_0} \left(\frac{a}{l}\right)^2 = \frac{u_0}{2D} \quad (42)$$

is a dimensionless parameter characterizing the strength of the exciton-exciton interaction. As can be seen from Eq. (42), the magnitude of  $G$  can be tuned by varying the magnetic field:  $G$  increases with decreasing the magnetic length  $l$ . Note also that the logarithmic frequency dependence of  $Q(\omega)$  is similar to that of the exciton-exciton scattering matrix.<sup>67,64</sup>

In the following, we will distinguish between attractive and repulsive exciton-exciton interactions.

### A. Attractive interaction

We first consider the case of attractive exciton-exciton interactions, corresponding to  $G > 0$ . For  $\omega < 2\Omega_0$ , the imaginary part of  $Q(\omega)$  vanishes and the memory function  $S(\omega)$  exhibits a biexciton pole. In the case of weak exciton-exciton interaction (weak asymmetry), the corresponding frequency  $\omega_b$  can be determined by using the low-frequency asymptotics (41) of  $Q(\omega)$ :  $1 - G \ln \left| \frac{2D}{\omega_b - 2\Omega_0} \right| = 0$ . This gives

$$\omega_b = 2\Omega_0 - E_b, \quad E_b = 2De^{-1/G}, \quad (43)$$

where  $E_b$  is the biexciton binding energy. Note that the above expression holds for  $G \ll 1$  corresponding to small biexciton energy  $E_b \ll D$ . The biexciton contribution to  $S(\omega)$  can be obtained by expanding Eq. (41) in the vicinity of  $\omega_b$ :

$$S_b(\omega) \sim -\frac{E_b}{G} \frac{1}{\omega - 2\Omega_0 + E_b + i\gamma_b}, \quad (44)$$

or, in the time domain,

$$S_b(t) = \frac{iE_b}{G} \theta(t) e^{i(E_b - 2\Omega_0)t - \gamma_b t}, \quad (45)$$

where  $\theta(t)$  is the step function and we have included the biexciton width  $\gamma_b$  that mainly comes from electron-phonon processes not incorporated in the Hamiltonian  $H$  considered here.

In the time domain, the biexciton resonance leads to oscillations of the memory kernel with a period determined by the biexciton binding energy (see Eq. (45)). The memory effects decay on a time scale determined by the *biexciton* dephasing time, which, in a magnetic field, can be considerably *longer* than the exciton dephasing time.<sup>62,63</sup> Near the biexciton resonance, the amplitude  $\chi(\omega)$  [see Eq. (35)] that determines the FWM signal, takes the form

$$\chi_b(\omega) = G^{-1} \frac{V^{HF} p^{(2)}(\omega)}{\omega - 2\Omega_0 + E_b + i\gamma_b}, \quad (46)$$

and exhibits a biexciton pole as a function of frequency.

The memory function  $S(\omega)$  also exhibits a second resonance centered at the frequency  $\omega_{sc} = 2\Omega_0 + E_b$ , which describes the continuum band of exciton-exciton scattering states. The width of this broad continuum resonance is determined by the exciton-exciton interactions. Indeed, for  $\omega > 2\Omega_0$ , the function  $Q(\omega)$ , that describes the exciton-exciton scattering, develops an imaginary part proportional to the interaction strength [see Eq. (41)]. For  $E_b > \gamma_b$ , the scattering band and biexciton resonance are well separated from each other and lead to distinct dynamics, while for  $E_b < \gamma_b$  they merge into a single asymmetric peak.

The above results hold in the case of weak exciton-exciton scattering,  $G \ll 1$ . With increasing magnetic field, the parameter  $G$ , Eq. (42), that characterizes the strength of the exciton-exciton interaction increases, and so does the biexciton binding energy  $E_b$ . For sufficiently strong magnetic fields such that  $E_b \gg D$ , corresponding to  $G \gg 1$ , one can use the high frequency asymptotic expansion of  $Q(\omega)$ , Eq. (40), which when substituted into Eqs. (36) and (35) gives

$$\chi(\omega) = \frac{V^{HF} p^{(2)}(\omega)}{\omega - 2\Omega_0 + u_0 + i\gamma_b}. \quad (47)$$

Note that for  $G \sim 1$ , we have  $E_b \sim u_0$ , and Eqs. (47) and (46) match.

It is important to note that Eq. (47) becomes exact in the strong field limit,  $l \ll a$ . Indeed, in this case, the typical magnetoexciton momenta are small,  $q \sim a^{-1} \ll l^{-1}$ , so that

one can disregard the magnetoexciton dispersion in Eq. (34) and replace  $\Omega_q$  by  $\Omega_0$ , which leads again to Eq. (40) for  $Q(\omega)$  and, therefore, to Eq. (47) for  $\chi(\omega)$ . In other words, for  $G \gg 1$ , the exciton-exciton scattering is suppressed and the memory effects are dominated by the biexciton resonance. The simple expression (47) can be then viewed as a “biexciton pole approximation” for the two-exciton amplitude  $\chi(\omega)$ . In fact, Eq. (47) is equivalent to the average polarization model<sup>12,70,25,1,63</sup> (APM), as we show in Appendix D.

In Fig. (1) we plot the memory function, obtained by evaluating Eqs. (36) and (34) with the full exciton dispersion (7). As we can see, for attractive interaction,  $S(\omega)$  is mainly dominated by the biexciton pole.

## B. Repulsive interaction

Let us now turn to the case of repulsive exciton-exciton interactions,  $G < 0$ . In this case, the memory function describes a continuum band of scattering states above the two-exciton energy. We start with the case of strong interactions  $|G| \gg 1$ . Here we can use again the high frequency asymptotics (40) for  $\text{Re}Q(\omega)$  (valid for  $\omega - 2\Omega_0 \gg D$ ). We see from Eq. (36) that  $S(\omega)$  exhibits a resonance at  $\omega = 2\Omega_0 + |u_0|$ . In contrast to the attractive case however, in this frequency range  $Q(\omega)$  develops imaginary part, which can be deduced from Eq. (38) as  $\text{Im}Q(\omega) = -i\pi G e^{-(\omega - 2\Omega_0)/2D} \theta(\omega - 2\Omega_0)$ . Near the resonance, we obtain from Eqs. (36) and Eq. (35) that

$$\chi(\omega) = \frac{V^{HF} p^{(2)}(\omega)}{\omega - 2\Omega_0 - |u_0| + i\gamma_{sc}}, \quad \gamma_{sc} = \pi u_0 G e^{-|G|}. \quad (48)$$

The above expression describes a resonance made up from the continuum of scattering states. Eq. (48) is valid for  $|u_0|/2D = |G| \gg 1$ , indicating that in this case the resonance is sharp. Comparing to Eq. (48), we can view this continuum resonance as an antibound state. The crucial difference, however, is that here the resonance width  $\gamma_{sc}$  is determined by the exciton-exciton interactions rather than homogeneous broadening due to phonons. The narrow width of the resonance comes from the fact that for  $|G| \gg 1$ , the momentum exchange processes between excitons are suppressed. Note here that the APM (47) is equivalent to Eq. (48) but with  $\gamma_{sc}$  introduced phenomenologically.

With decreasing  $|G|$ , the lineshape of the memory function changes. This is illustrated in Fig. (2). The sharp Lorentzian peak transforms into a broad asymmetric band centered at lower frequencies. Importantly,  $S(\omega)$  develops a *cusp* at  $\omega = 2\Omega_0$ . This cusp is manifestation of the logarithmic singularity in the low-frequency asymptotics of  $Q(\omega)$  [see Eq. (41)]. In the next section we will see that this low-frequency behavior of the memory function has a dramatic effect on the FWM polarization for long time delays.

## VI. NUMERICAL RESULTS AND DISCUSSION

In this section, we present the results of numerical calculations of the third-order FWM polarization and compare them to the analytical solution of Sec. IV and V. The calculations below also incorporate the Pauli blocking contribution,  $\tilde{P}_{PB}(t, \tau)$ , to the total FWM polarization  $\tilde{P}(t, \tau) = \tilde{P}_{XX}(t, \tau) + \tilde{P}_{PB}(t, \tau)$ , which is given in Appendix C. We use the standard

conventions according to which the positive time-delay,  $\tau > 0$ , corresponds to probe pulse arriving before the pump pulse. We will be interested mainly in the time-integrated and spectrally-resolved FWM signals, defined as

$$\text{TI-FWM} = \int_{-\infty}^{\infty} dt |\tilde{P}(t, \tau)|^2 \quad (49)$$

and

$$\text{SR-FWM} = |\tilde{P}(\omega, \tau)|^2, \quad (50)$$

respectively, where  $\tilde{P}(\omega, \tau)$  is the Fourier transform of  $\tilde{P}(t, \tau)$ .

### A. Attractive interaction

We start with the case of attractive exciton-exciton interactions,  $u_0 > 0$ . In Fig. 3 we show the results of our numerical calculation of the TI-FWM signal for a strong magnetic field,  $a/l = 6.0$ , and for both strong and weak  $e$ - $h$  asymmetry. In order to be consistent with the recent experimental data,<sup>62,63</sup> we have chosen the biexciton homogeneous broadening,  $\gamma_b$ , to be smaller than that of the exciton,  $\Gamma$ . In both cases, the calculations yield a strong TI-FWM signal at negative time delays. For strong asymmetry (large  $u_0$ ), the biexciton oscillator strength in the memory function  $S(\omega)$  is enhanced (see Fig. (1)), and the TI-FWM signal exhibits biexciton oscillations. This behavior can be easily deduced from the analytic results of the previous section. Indeed, for  $\delta$ -function pump pulse centered at  $t = 0$ , the pump polarization (24) is given by  $p(t) = -i\mu\mathcal{E}_2\theta(t)e^{-i\Omega_0 t - \Gamma t}$ , and the biexciton contribution to the amplitude  $\chi(t)$  [Eq. (46)] takes the simple form

$$\chi_b(t) = \frac{\theta(t)e^{-2i\Omega_0 t}(\mu\mathcal{E}_2)^2}{G[E_b - i(2\Gamma - \gamma_b)]} \left( e^{iE_b t - \gamma_b t} - e^{-2\Gamma t} \right). \quad (51)$$

The first term in the rhs leads to the oscillations in the TI-FWM signal with the period  $T_b = 2\pi/E_b$ , and to the overall exponential decay of the TI-FWM signal with the characteristic time  $\gamma_b^{-1}$  at long negative time delays. Such a behavior is also consistent with the calculations in Ref. 65.

In Fig. 4, we plot the time evolution of the corresponding SR-FWM signal, which shows both an exciton and a (weaker) biexciton peak. A distinguishing feature of the spectra is that the height of the *exciton* peak oscillates as a function of time delay with a period determined by the *biexciton* binding energy,  $T_b = 2\pi/E_b$ . This behavior is easily reproduced by using Eq. (51) (see below).

As mentioned in the previous section, in the strong magnetic field case  $l/a \ll 1$ , the exciton-exciton scattering is suppressed and the FWM polarization is governed by the biexcitonic effects. In Fig. 5, we show the TI-FWM signal for weaker magnetic field such that  $a/l = 3.0$  and for two different pump durations, both of which are shorter than the exciton dephasing time,  $t_0 < \Gamma^{-1}$ . In Fig. 5(a), the pulse duration was chosen to be shorter than the inverse biexciton energy,  $t_0 < E_b^{-1}$ . In this case, the TI-FWM curves are qualitatively similar to those in Fig. 3(a); in particular, they exhibit an overall exponential decay at long negative time delays together with biexciton oscillations as  $u_0$  increases. In contrast, for

the longer pulse duration  $t_0 > E_b^{-1}$ , the change in the shape of the TI-FWM signal with increasing  $u_0$  is different [see Fig. 5(b)].

To understand this behavior, we note that, for weak asymmetry  $u_0/E_0 \ll 1$ , we have  $t_0 < E_b^{-1}$ , and the decay of the TI-FWM signal is similar to that for the shorter pulse duration [compare Figs. 5(b) and 5(a)]. On the other hand, for larger  $u_0$  we have  $t_0 > E_b^{-1}$ , and the pump pulse tuned at the magnetoexciton level,  $\Omega_0 = 0$ , does not directly excite the biexciton. In this case the decay at intermediate times becomes non-exponential, while the amplitude of the oscillations is significantly enhanced [see Fig. 5(b)]. The reason for such a behavior is that, for short time delays, the signal decays exponentially with the Hartree-Fock decay time<sup>12</sup>  $(4\Gamma)^{-1}$  [see Fig. 3(b)], while for longer time delays, the build-up of the biexciton correlations leads to an exponential decay with a different characteristic time,  $(2\gamma_b)^{-1}$ , determined by the biexciton width. The crossover between these two regimes leads to an apparent nonexponential decay at intermediate time delays [see Fig. 3(b)].

The sensitivity to the detuning of the time-evolution of the FWM polarization becomes even more evident in the SR-FWM signal. In Figs. 6 and 7, we plot the corresponding spectra versus time delay for pump tuned to the exciton and biexciton levels, respectively. For  $\Omega_0 = 0$ , the exciton peak decays exponentially for positive time delays,  $\tau > 0$ , with characteristic time  $(2\Gamma)^{-1}$ , while the biexciton peak is suppressed (see Fig. 6). For pump tuned at the biexciton,  $2\Omega_0 = E_b$ , the situation changes: for  $\tau > 0$  the decay of the exciton peak follows the pump pulse, while the biexciton peak decays exponentially with a characteristic time  $(2\Gamma)^{-1}$  (see Fig. 7). For negative time delays, the exciton peak oscillates with the period  $2\pi/E_b$  (compare to Fig. 4).

To understand this behavior, consider the biexciton contribution to the frequency-dependent polarization  $\tilde{P}_{XX}(\omega, \tau)$ . The latter can be presented as a sum of two terms  $\tilde{P}_b^{(1)}(\omega, \tau) + \tilde{P}_b^{(2)}(\omega, \tau)$ , corresponding to the first and second terms in Eq. (19). The first term can be presented as

$$\tilde{P}_b^{(1)}(\omega, \tau) = -\frac{\mu^2 \mathcal{E}_1 e^{i(\bar{\omega} + \Omega_0)\tau} \chi_b(-\tau)}{\bar{\omega} + i\Gamma}, \quad (52)$$

where  $\bar{\omega} = \omega - \bar{E}_g + E_0$  is the frequency measured from the magnetoexciton level (we used here that  $\Omega_0 = \bar{E}_g - E_0 - \omega_0$ ). Equation (52) describes the peak at the exciton energy,  $\bar{\omega} = 0$ . The peak height depends on the time delay via  $\chi_b(-\tau)$ . The latter, for short pulse duration, can be approximated by Eq. (51), leading, for  $\tau < 0$ , to the oscillations of the exciton peak amplitude with the period  $2\pi/E_b$  determined by the biexciton binding energy (see Figs. 4 and 5). Note that, since  $\chi_b(t) = 0$  for times  $t < 0$  prior to the onset of the pump pulse [see Eq. (51)], the above contribution vanishes for  $\tau > 0$ . Therefore, for positive time delays, the SR-FWM signal at the exciton frequency is primarily determined by the Pauli blocking term.

The second term in Eq. (19) has the form

$$\tilde{P}_b^{(2)}(\omega, \tau) = \mu^2 \mathcal{E}_1 e^{-i(\bar{\omega} + \Omega_0)\tau} \int_{-\infty}^{\infty} \frac{d\omega'}{2\pi} \frac{e^{i\omega'\tau} \chi_b(\omega')}{\bar{\omega} + 2\Omega_0 - \omega' + i\Gamma}. \quad (53)$$

Using Eq. (46), the integrand of Eq. (53) can be decomposed as

$$\frac{\chi_b(\omega')}{\bar{\omega} + 2\Omega_0 - \omega' + i\Gamma} = \frac{G^{-1} V^{HF} p^{(2)}(\omega')}{\bar{\omega} + E_b + i(\Gamma + \gamma_b)} \left[ \frac{1}{\omega' - 2\Omega_0 + E_b + i\gamma_b} + \frac{1}{\bar{\omega} + 2\Omega_0 - \omega' + i\Gamma} \right], \quad (54)$$

yielding

$$\tilde{P}_b^{(2)}(\omega, \tau) = \frac{\mu^2 \mathcal{E}_1 G^{-1} e^{-i(\omega + \Omega_0)\tau}}{\bar{\omega} + E_b + i(\Gamma + \gamma_b)} \int_{-\infty}^{\infty} \frac{d\omega'}{2\pi} \left[ \frac{V^{HF} p^{(2)}(\omega') e^{i\omega'\tau}}{\omega' - 2\Omega_0 + E_b + i\gamma_b} + \frac{V^{HF} p^{(2)}(\omega') e^{i\omega'\tau}}{\bar{\omega} + 2\Omega_0 - \omega' + i\Gamma} \right]. \quad (55)$$

The prefactor in the rhs of Eq. (55) has a resonance at the biexciton frequency,  $\bar{\omega} = -E_b$ , with width  $\Gamma + \gamma_b$ . The amplitude of the biexcitonic peak is determined by the integral in Eq. (55). For negative delays, the main contribution to the above integral comes from the first term in the integrand, whose denominator has a pole at  $\omega' = 2\Omega_0 - E_b$ . For resonant pump excitation,  $\Omega_0 = 0$ , and pulse duration  $t_0 < \Gamma^{-1}$ , the frequency width of  $p^{(2)}(\omega')$  in the integrand of Eq. (55) is of the order of  $2\Gamma$ . In this case, the contribution of the pole is suppressed for  $E_b > \Gamma$ , and therefore the biexciton peak is diminished (see Fig. 6). For off-resonant pump tuned at the biexciton,  $2\Omega_0 \simeq E_b$ , and for pulse duration  $t_0 > 2/E_b \sim \Omega_0^{-1}$ , the time dependence of  $p(t)$  is mainly determined by that of the pulse itself, so that the frequency width of  $p^{(2)}(\omega')$  is  $\sim t_0^{-1}$ . In this case the pole dominates the integral, leading to a strong biexciton peak in the SR-FWM signal, which decays on a time scale  $(2\gamma_b)^{-1}$  (see Fig. 7).

For positive delays,  $\tau > 0$ , the main contribution to the biexciton term  $\tilde{P}_b^{(2)}(\omega, \tau)$  comes from the second term of the integrand in Eq. (55), which exhibits a pole at  $\omega' = \bar{\omega} + 2\Omega_0$ . Since  $\bar{\omega} \sim -E_b$  due to the prefactor in Eq. (55), for resonant excitation,  $\Omega_0 = 0$ , the biexciton peak is diminished for  $E_b > \Gamma$  (see Fig. 6). For off-resonant excitation,  $2\Omega_0 = E_b$ , this pole dominates the integral leading to a strong SR-FWM signal at the biexciton energy (see Fig. 7), which decays on a time scale  $(2\Gamma)^{-1}$  [see Eq. (55)]. Note that, for pump excitation at the *biexciton* frequency,  $2\Omega_0 = E_b$ , the SR-FWM signal at the *exciton* frequency is strong for negative time delays due to the exciton-exciton correlations [see Eq. (52)], but diminishes after the pump pulse is gone due to the suppression of both the Pauli blocking contribution and  $\tilde{P}_b^{(1)}$  [see Eq. (52)].

It should be noted that for all the above parameter values, the analytical curves calculated from Eqs. (34-36), which were derived in the previous section for  $l < a$ , are practically indistinguishable from the exact numerical calculations in Figs. 3-7. In fact, Eqs. (34-36) provide a very good approximation even for  $a \sim l$ . This is demonstrated in Fig. 8, where we present the results of numerical calculations of the TI-FWM signal at  $a/l = 1.5$  together with the analytic solution (34-36) for different values of the biexciton width  $\gamma_b$ . For comparison, we also plot the TI-FWM signal derived using the APM (47). Note that, for the parameters used in Fig. 8,  $u_0/D \sim 5.0$  and we are therefore in a regime where Eq. (47) is meaningful. We see that our analytic solution (35), which includes the effects of the exciton-exciton scattering processes, neglected by the APM, is in a much better agreement with the numerical results even for strong  $e$ - $h$  asymmetry. In particular, the APM (47) fails to provide the correct period and amplitude of the biexciton oscillations for both  $\gamma_b \ll \Gamma$  or  $\gamma_b = 2\Gamma$ . In addition, the APM gives a considerably weaker magnitude of the FWM signal.

## B. Repulsive interaction

Let us now turn to repulsive exciton-exciton interactions,  $u_0 < 0$ . In Fig. 9, we show the TI-FWM signal in a strong magnetic field,  $a/l = 3.0$ , for several values of the parameter

$G$  [Eq. (42)] characterizing the strength of the exciton-exciton interactions. For large  $|G|$ , the signal decays exponentially with a characteristic time that increases with  $|G|$ . In this regime, the memory function  $S(\omega)$  is dominated by an antibound state well separated from the exciton resonance (see Fig. 2). A narrow antibound resonance leads to oscillations in the TI-FWM signal, similar to biexciton oscillations. Note that antibound states were recently observed experimentally in the FWM signal of QW's at zero magnetic field.<sup>71</sup> The decay time is simply the inverse antiresonance width, given by Eq. (48). Importantly, the latter is determined by the exciton-exciton interactions, consistent with Fig. 9.

As  $|G|$  decreases, we observe a transition from an exponential regime for initial time delays, where the antiresonance dominates the decay, to a *nonexponential* regime for long negative time delays. For small  $|G|$ , the latter regime extends down to times  $\sim 2/\Gamma$ ; for longer times, the TI-FWM signal curves up with increasing  $|\tau|$  (see Fig. 9).

The long nonexponential tail of the TI-FWM signal has its origin in the low-frequency behavior of the memory function  $S(\omega)$ . As can be seen from Eq. (19), the shape of the signal for long negative delays is determined by the long-time asymptotics of the amplitude  $\chi(t)$ . The latter can be derived by using the analytic expression (35) for  $\chi(\omega)$ . For sufficiently large  $t$ , we can substitute into Eq. (35) the low-frequency asymptotics of the memory function  $S(\omega)$  [see Eq. (41)],

$$S(\omega) \simeq \frac{1}{1 + |G| \ln \left| \frac{2D}{\omega - 2\Omega_0} \right| + i\pi |G| \theta(\omega - 2\Omega_0)}. \quad (56)$$

As shown in Appendix E, for short pump duration this gives

$$\chi(t) \simeq \frac{i(\mu\mathcal{E}_2)^2}{2\Gamma} \frac{e^{-2i\Omega_0 t} V^{HF}}{1 + |G| \ln 2Dt}, \quad (57)$$

with  $D$  given by Eq. (39). The above result is valid for long times  $t \gg D^{-1}$ . The slow logarithmic decay of the amplitude  $\chi(t)$  reflects the singular behavior of  $S(\omega)$  at small frequencies. Note that *both* the real and the imaginary part of the memory function (56) contribute to the asymptotics (57) (see Appendix E).

Using Eqs. (57) and (19), the TI-FWM signal (49) for negative time delay takes the form

$$\text{TI-FWM} = \frac{\mu^6 \mathcal{E}_2^4 \mathcal{E}_1^2}{4\Gamma^2} V^{HF} \int_{|\tau|}^{\infty} dt e^{-2\Gamma(t-|\tau|)} \left( \frac{1}{1 + |G| \ln 2D|\tau|} - \frac{1}{1 + |G| \ln 2Dt} \right)^2. \quad (58)$$

The main contribution to the integral comes from times  $(t - |\tau|) \lesssim \Gamma^{-1}$ . For  $|\tau| \gg \Gamma^{-1}$ , the second term in the rhs of Eq. (58) can be expanded in  $(t - |\tau|)/|\tau|$ , and we finally obtain

$$\text{TI-FWM} \propto \frac{G^2}{\Gamma^5} \frac{(V^{HF})^2}{\tau^2 (1 + |G| \ln 2D|\tau|)^4}. \quad (59)$$

The above expression describes the long tail of the TI-FWM signal for negative time delays in Fig. 9. Note that Eq. (59) is valid for  $|\tau| \gg \Gamma^{-1}$ , so that with increasing  $\Gamma$ , the crossover to the asymptotic behavior (59) occurs at earlier time delays, as can be seen in Fig. 9(b).

The behavior of the TI-FWM signal on various time scales can be tuned by changing the magnetic field strength. For strong magnetic fields  $l \ll a$ , the momentum exchange processes



between excitons are suppressed and the TI-FWM signal is dominated by the antibound state resonance leading to the exponential decay. With decreasing magnetic field, the energy scale  $D$  which determines the characteristic exciton momenta  $q \sim (2MD)^{1/2}$ , increases [see Eq. (39)], and the crossover to the above nonexponential regime occurs at earlier times  $|\tau| > D^{-1}$  [see Figs. 10(a) and 11(a)]. At the same time, the shape of the TI-FWM signal for  $|\tau| > D^{-1}$  depends strongly on  $G$ . For  $|G| \sim 1$ , the decay is described by the equation

$$\text{TI-FWM} \propto \frac{(V^{HF})^2}{\Gamma^5 G^2} \frac{1}{\tau^2 (\ln 2D|\tau|)^4}. \quad (60)$$

For  $|G| \ll 1$ , the situation is more intricate. In this case, the asymptotics (60) applies for very long time delays,  $|\tau| \gtrsim D^{-1} e^{\frac{1}{|G|}} \gg D^{-1}$ , while for  $D^{-1} \lesssim |\tau| \lesssim D^{-1} e^{\frac{1}{|G|}}$  the decay is quadratic.

The behavior of the TI-FWM signal at initial times,  $|\tau| \lesssim D^{-1}$ , is mainly determined by the imaginary part of  $S(\omega)$ . At small  $|G|$ , the memory function is a smooth function of frequency for  $\omega \gtrsim D$  (see Fig. 2), and, correspondingly,  $S(t)$  is nearly instantaneous, so that the TI-FWM signal shows a Hartree-Fock-like decay (see curves with  $|G| = 0.24$  in Fig. 9). At  $|G| \sim 1$ ,  $\text{Im}S(\omega)$  represents a broad asymmetric peak centered at  $E_{sc} \sim u_0$  with the width  $\gamma_{sc} \sim D$ , so that TI-FWM signal exhibits weak oscillations and overall exponential decay on time scale  $|\tau| \sim D^{-1}$ . For long time delays,  $|\tau| \gtrsim D^{-1}$ , the low-frequency singular behavior of the memory functions becomes important and the crossover to the asymptotic regime Eq. (59) occurs (see curves with  $|G| = 1.2$  in Fig. 9). For larger  $|G|$ , the crossover occurs at even longer times,  $|\tau| \gg D^{-1}$  (see curves with  $|G| = 3.6$  in Fig. 9).

In Figs. 10 and 11 we compare the numerically calculated TI-FWM signal with the analytic solution (34-36) and with the APM (48). In the latter case, the width of the band of exciton-exciton scattering states,  $\gamma_{sc}$ , must be introduced phenomenologically by fitting the memory function  $S(\omega)$  with a Lorentzian [see Figs. 10(b) and 11(b)]. Even though such an approximation describes well the overall lineshape of the memory function, the latter deviates from a Lorentzian in the low frequency domain. These discrepancies have a profound effect on the TI-FWM signal. Namely, even though in the initial exponential regime the APM and numerical curves are in a reasonable agreement with each other, the APM completely fails to reproduce the long nonexponential tail of the TI-FWM signal. The latter originates from the singular low-frequency behavior of  $S(\omega)$  [see Eq. (56)]. On the other hand, the analytic solution (34-36) describes accurately the long nonexponential tail of the TI-FWM signal as well as the crossover between the two regimes [see Figs. 10(a) and 11(a)].

## VII. CONCLUSIONS

In summary, we studied the role of the exciton-exciton interactions in the ultrafast nonlinear optical spectroscopy of semiconductor quantum wells in a perpendicular magnetic field. In the case of attractive exciton-exciton interactions, we found that the biexcitonic effects dominate. For repulsive interaction, we have shown that the time-integrated four-wave-mixing signal exhibits a long nonexponential tail for negative time delays. We traced the origin of this tail to the low-frequency of the memory kernel for the two-exciton wavefunction, for which we derive an explicit analytical expression.

Our analytical solution, given by Eqs. (34-36), was derived here in the case of strong magnetic field, where the kinetic energy of the electrons and holes is frozen and the exciton-exciton interactions play a dominant role in the third-order optical response. We believe, however, that Eqs. (34-36) can serve as an analytical model also for the zero magnetic field case, for example, when the dynamics is dominated by interactions of 1s excitons. In particular, our solution reproduces, as a limiting case, the well-known average polarization model,<sup>12,70,25,1,63</sup> which has been used in the case of zero magnetic field. Unlike the APM, however, the model (34-36) takes into account nonperturbatively the correlation effects due to the *continuum* of exciton-exciton scattering states.

## ACKNOWLEDGMENTS

We thank D. S. Chemla for useful discussions. This work was supported by the NSF grant ECS-9703453.

## APPENDIX A:

In this appendix, we present a general expression for the third-order FWM polarization derived using the canonical-transformation formalism.<sup>46,47,49</sup> The total Hamiltonian of the system is  $H_{tot} = H + H_p + H_s$ , where  $H$  is the two-band semiconductor Hamiltonian (considered in the rotating frame from now on) and  $H_\alpha$  describe the coupling to the optical fields ( $\alpha = 1, 2$  for probe and pump, respectively),

$$H_\alpha = -M_\alpha(t)U^\dagger + \text{H.c.} \quad (\text{A1})$$

with

$$M_\alpha(t) = e^{i\mathbf{k}_\alpha \mathbf{r} - i\omega_0 t} \mu \mathcal{E}_\alpha(t), \quad U^\dagger = \sum_{\mathbf{k}} a_{\mathbf{k}}^\dagger b_{-\mathbf{k}}^\dagger. \quad (\text{A2})$$

Here  $U^\dagger$  is the optical transition operator,  $a_{\mathbf{k}}^\dagger$  and  $b_{-\mathbf{k}}^\dagger$  are the creation operators for electron and hole respectively with momentum  $\mathbf{k}$ ;  $\mathcal{E}_\alpha(t)$  are the amplitudes of the optical fields propagating in the probe ( $\mathbf{k}_1$ ) and pump ( $\mathbf{k}_2$ ) directions with central frequency  $\omega_0$ , and  $\mu$  is the dipole matrix element.

The nonlinear optical polarization is given by  $P(t) = \mu \langle \Psi(t) | U | \Psi(t) \rangle$ , where the state  $|\Psi(t)\rangle$  satisfies the Schrödinger equation with Hamiltonian  $H_{tot}$ . The third-order polarization propagating along the FWM direction  $2\mathbf{k}_2 - \mathbf{k}_1$  can be obtained by expanding the state  $|\Psi(t)\rangle$  to the first order in the probe and second order in the pump field. The FWM polarization then takes the form  $P_{FWM}(t) = e^{i(2\mathbf{k}_2 - \mathbf{k}_1) \cdot \mathbf{r}} \tilde{P}(t)$  with<sup>47,46</sup>

$$\tilde{P}(t) = i\mu^2 e^{-i\omega_0 t} \int_{-\infty}^t dt' \mathcal{E}_1^*(t') \left[ \langle 0 | U e^{-iH(t-t')} U_{FWM}^\dagger(t') | 0 \rangle - (t \leftrightarrow t') \right]. \quad (\text{A3})$$

The above expression has a form similar to the linear polarization due to the probe optical field, with the important difference that here the single  $e$ - $h$  pair state  $U_{FWM}^\dagger(t)|0\rangle$  depends on the pump optical field,

$$U_{FWM}^\dagger|0\rangle = UW^\dagger|0\rangle - \mathcal{P}^\dagger U\mathcal{P}^\dagger|0\rangle, \quad (\text{A4})$$

where  $|0\rangle$  is the ground state of  $H$ . Here the states  $\mathcal{P}^\dagger(t)|0\rangle$  and  $W^\dagger(t)|0\rangle$  are the first and second order terms of the expansion of the state  $|\Phi(t)\rangle$  that evolves from the semiconductor ground state under photoexcitation by the *pump alone*,

$$|\Phi(t)\rangle \propto |0\rangle - e^{i\mathbf{k}_2 \cdot \mathbf{r}}\mathcal{P}^\dagger(t)|0\rangle + e^{2i\mathbf{k}_2 \cdot \mathbf{r}}W^\dagger(t)|0\rangle. \quad (\text{A5})$$

The *single e-h* pair state  $\mathcal{P}^\dagger(t)|0\rangle$  and the *two e-h* pair state  $W^\dagger(t)|0\rangle$  excited by the pump optical field satisfy the equations

$$i\partial_t\mathcal{P}^\dagger(t)|0\rangle = H\mathcal{P}^\dagger(t)|0\rangle + \mu\mathcal{E}_2(t)U^\dagger|0\rangle, \quad (\text{A6})$$

and

$$i\partial_tW^\dagger(t)|0\rangle = HW^\dagger(t)|0\rangle + \mu\mathcal{E}_2(t)U^\dagger\mathcal{P}^\dagger(t)|0\rangle, \quad (\text{A7})$$

respectively.<sup>47,46</sup>

The decomposition (A4) has a straightforward interpretation. The first term in the rhs describes the FWM signal coming from the excitation of two *e-h* pairs by the pump followed by the de-excitation of one pair by the probe. The second term describes the excitation of an *e-h* pair by the pump, followed by de-excitation by the probe and then excitation of an *e-h* pair by the pump again. The first term in Eq. (A4) describes the two-exciton contribution to the FWM signal, while the second term describes the one-exciton contribution. Note that, in a two-level system, only the second term in Eq. (A4) is present.

## APPENDIX B:

Starting from the general formulae in Appendix A, we derive here a simple expression for the FWM signal coming from the exciton-exciton interactions. The Pauli blocking contribution is outlined in Appendix C.

Equation (A7) describes the time evolution of the two-exciton state from an initial state of two *non-interacting* excitons photoexcited by the pump. It is useful to separate out the contribution  $W_0^\dagger(t)|0\rangle$  due to non-interacting excitons with zero momentum by writing  $W^\dagger(t)|0\rangle = W_0^\dagger(t)|0\rangle + W_{XX}^\dagger(t)|0\rangle$ , where the second term comes from the exciton-exciton interactions. In the following we assume that the photoexcited electrons and holes are confined to their respective LLL's, so that the energy of two noninteracting magnetoexcitons with zero momentum is simply  $2\Omega_0$ , where  $\Omega_0$  is the pump detuning from the zero-momentum exciton energy (we work in the rotating frame).

The time evolution of the non-interacting exciton state is determined by the equation

$$i\partial_tW_0^\dagger(t)|0\rangle = 2\Omega_0W_0^\dagger(t)|0\rangle + \mu\mathcal{E}_2(t)U^\dagger\mathcal{P}^\dagger(t)|0\rangle. \quad (\text{B1})$$

After subtracting Eq. (B1) from Eq. (A7), we obtain that the exciton-exciton interactions are described by the time-dependent Schrödinger-like equation

$$i\partial_tW_{XX}^\dagger(t)|0\rangle = HW_{XX}^\dagger(t)|0\rangle + (H - 2\Omega_0)W_0^\dagger(t)|0\rangle. \quad (\text{B2})$$

The source term on the rhs is the Hartree-Fock interaction between two zero-momentum excitons. The exciton-exciton correlations come from the Coulomb potential in the Hamiltonian  $H$  (first term in the rhs of Eq. (B2)).

Thus, we can present Eq. (A4) as a sum of two contributions:

$$U_{FWM}^\dagger|0\rangle = U_{PB}^\dagger|0\rangle + U_{XX}^\dagger|0\rangle, \quad (\text{B3})$$

where

$$U_{PB}^\dagger(t)|0\rangle = UW_0^\dagger|0\rangle - \mathcal{P}^\dagger U \mathcal{P}^\dagger|0\rangle \quad (\text{B4})$$

describes the Pauli blocking effects for noninteracting excitons, and

$$U_{XX}^\dagger(t)|0\rangle = UW_{XX}^\dagger|0\rangle \quad (\text{B5})$$

comes from the exciton-exciton interactions. The polarization (A3) can then be presented as a sum of Pauli blocking and exciton-exciton interaction parts,  $\tilde{P}(t) = \tilde{P}_{PB}(t) + \tilde{P}_{XX}(t)$ , where

$$\begin{aligned} \tilde{P}_{PB}(t) &= i\mu^2 e^{-i\omega_0 t} \int_{-\infty}^t dt' \mathcal{E}_1^*(t') \left[ \phi_{PB}(t, t') - \phi_{PB}(t', t) \right], \\ \tilde{P}_{XX}(t) &= i\mu^2 e^{-i\omega_0 t} \int_{-\infty}^t dt' \mathcal{E}_1^*(t') \left[ \phi_{XX}(t, t') - \phi_{XX}(t', t) \right], \end{aligned} \quad (\text{B6})$$

with

$$\begin{aligned} \phi_{PB}(t, t') &= \langle 0 | U e^{-iH(t-t')} U_{PB}^\dagger(t') | 0 \rangle, \\ \phi_{XX}(t, t') &= \langle 0 | U e^{-iH(t-t')} U_{XX}^\dagger(t') | 0 \rangle. \end{aligned} \quad (\text{B7})$$

Equations (B6) provide an exact formal expression for the third-order FWM signal.

Here we focus on the the interaction-induced FWM polarization, and defer the Pauli blocking contribution to Appendix C.  $\tilde{P}_{XX}(t)$  is determined by the correlation function  $\phi_{XX}(t, t')$ , which satisfies the equation

$$i\partial_t \phi_{XX}(t, t') = \langle 0 | U H e^{-iH(t-t')} U_{XX}^\dagger(t') | 0 \rangle \quad (\text{B8})$$

with the initial condition  $\phi_{XX}(t, t) = \chi(t)$ , where

$$\chi(t) = \langle 0 | U U_{XX}^\dagger(t) | 0 \rangle = \langle 0 | U U W_{XX}^\dagger(t) | 0 \rangle. \quad (\text{B9})$$

Since the state  $U^\dagger|0\rangle = N^{1/2}d_0^\dagger|0\rangle$  is an eigenstate of  $H$  [see Eq. (9)], we obtain from Eq. (B8) that

$$\phi_{XX}(t, t') = e^{-i\Omega_0(t-t') - \Gamma|t-t'|} \chi(t'), \quad (\text{B10})$$

where  $\Gamma$  is the *exciton* homogeneous broadening. Since Eq. (B10) is linear in the probe optical field, we consider for simplicity a  $\delta$ -function probe  $\mathcal{E}_1(t) = e^{-i\omega_0 t} \mathcal{E}_1 \delta(t + \tau)$ . Substituting this into Eq. (B7) we obtain

$$\tilde{P}_{XX}(t, \tau) = i\mu^2 \mathcal{E}_1 \theta(t + \tau) e^{-\Gamma(t+\tau) - i\omega_0(t-\tau)} \left[ e^{-i\Omega_0(t+\tau)} \chi(-\tau) - e^{i\Omega_0(t+\tau)} \chi(t) \right]. \quad (\text{B11})$$

Using Eq. (12),  $\chi(t)$  can be expressed in terms of the coefficients of the expansion of the state  $W_{XX}^\dagger(t)|0\rangle$  in the two-exciton basis (11),

$$w_p(t) = \langle \mathbf{p}, -\mathbf{p} | W_{XX}^\dagger(t) | 0 \rangle, \quad (\text{B12})$$

as follows:

$$\chi(t) = w_0 - \frac{1}{N} \sum_{\mathbf{p}} w_p = w_0 - \tilde{w}_0. \quad (\text{B13})$$

The two terms in the rhs of Eq. (B13) reflect the two possible ways of arranging four particles into two excitons. The equation for the amplitude  $w_p(t)$  follows from Eq. (B2),

$$i\partial_t w_p(t) = \langle \mathbf{p}, -\mathbf{p} | H W_{XX}^\dagger(t) | 0 \rangle + \langle \mathbf{p}, -\mathbf{p} | (H - 2\Omega_0) W_0^\dagger(t) | 0 \rangle. \quad (\text{B14})$$

After projecting out the rhs of the above equation in the two-exciton basis Eq. (11) and using Eq. (16) for the matrix elements of  $H$ , Eq. (B14) takes the form

$$i\partial_t w_p(t) - 2\Omega_p w_p(t) = - \int \frac{d\mathbf{q}}{(2\pi)^2} V(\mathbf{p}, \mathbf{q}) w_q(t) + 2(\epsilon_p - \epsilon_0) w_p^0(t) - \int \frac{d\mathbf{q}}{(2\pi)^2} V(\mathbf{p}, \mathbf{q}) w_q^0(t), \quad (\text{B15})$$

where  $w_p^0(t) = \langle \mathbf{p}, -\mathbf{p} | W_0^\dagger(t) | 0 \rangle$  is the noninteracting two-exciton amplitude. The equation for the latter can be obtained straightforwardly from Eq. (B1):

$$i\partial_t w_p^0(t) - 2(\Omega_0 - i\Gamma) w_p^0(t) = \mu \mathcal{E}_2(t) \langle \mathbf{p}, -\mathbf{p} | U^\dagger \mathcal{P}^\dagger(t) | 0 \rangle. \quad (\text{B16})$$

In order to evaluate the last term in Eq. (B16), we use Eq. (A6) for the one-exciton state  $\mathcal{P}^\dagger(t)|0\rangle$  to obtain

$$(i\partial_t - \Omega_0 + i\Gamma) \langle \mathbf{p}, -\mathbf{p} | U^\dagger \mathcal{P}^\dagger(t) | 0 \rangle = \mu \mathcal{E}_2(t) \langle \mathbf{p}, -\mathbf{p} | U^\dagger U^\dagger | 0 \rangle. \quad (\text{B17})$$

Using Eqs. (10) and (12), we find that  $\langle \mathbf{p}, -\mathbf{p} | U^\dagger U^\dagger | 0 \rangle = N\delta_{\mathbf{p}0} - 1$ , so that

$$\langle \mathbf{p}, -\mathbf{p} | U^\dagger \mathcal{P}^\dagger(t) | 0 \rangle = (N\delta_{\mathbf{p}0} - 1) p(t) = \left[ \frac{2\pi}{l^2} \delta(\mathbf{p}) - 1 \right] p(t), \quad (\text{B18})$$

where  $p(t)$  is the linear pump-induced polarization, satisfying

$$i\partial_t p(t) = (\Omega_0 - i\Gamma) p(t) + \mu \mathcal{E}_2(t). \quad (\text{B19})$$

Substituting Eq. (B18) into Eq. (B16), and comparing the latter to Eq. (B19), we obtain that

$$w_p^0(t) = \left[ \frac{2\pi}{l^2} \delta(\mathbf{p}) - 1 \right] \frac{p^2(t)}{2}, \quad (\text{B20})$$

Substituting the above expression for  $w_p^0(t)$  into Eq. (B15) and using the decomposition  $V(\mathbf{p}, \mathbf{q}) = V_S(\mathbf{p}, \mathbf{q}) + V_A(\mathbf{p}, \mathbf{q})$  together with the relation (18), we arrive at the following equation for the two-exciton amplitude:

$$i\partial_t w_p(t) - 2\Omega_p w_p(t) = - \int \frac{d\mathbf{q}}{(2\pi)^2} V(\mathbf{p}, \mathbf{q}) w_q(t) + V_p^{HF} p^2(t), \quad (\text{B21})$$

where

$$V_p^{HF} = \frac{1}{2} \int \frac{d\mathbf{q}}{(2\pi)^2} V_A(\mathbf{p}, \mathbf{q}) - \frac{V_A(\mathbf{p}, 0)}{4\pi l^2}, \quad (\text{B22})$$

According to Eq. (B13), the amplitude  $\chi(t)$  is determined by the  $\mathbf{p} = 0$  solution of Eq. (B21) and by  $\tilde{w}_0(t) = N^{-1} \sum_{\mathbf{p}} w_p(t)$ . The equation for  $\tilde{w}_0(t)$  can be straightforwardly obtained by summing Eq. (B21) over all momenta  $\mathbf{p}$  and using the relation (18). This gives

$$i\partial_t \tilde{w}_0(t) - 2\Omega_0 \tilde{w}_0(t) = -\frac{1}{N} \sum_{\mathbf{p}} \int \frac{d\mathbf{q}}{(2\pi)^2} V_A(\mathbf{p}, \mathbf{q}) w_q(t) + \frac{1}{N} \sum_{\mathbf{p}} V_p^{HF} p^2(t). \quad (\text{B23})$$

Setting  $\mathbf{p} = 0$  in Eq. (B21), and subtracting from the latter Eq. (B23), we obtain a simple equation for the amplitude  $\chi(t)$  (Eq. (B13)) that determines the FWM polarization,

$$i\partial_t \chi(t) - 2\Omega_0 \chi(t) = V^{HF} p^2(t) + F(t), \quad (\text{B24})$$

where

$$V^{HF} = V_0^{HF} - \frac{l^2}{2\pi} \int d\mathbf{q} V_q^{HF} \quad (\text{B25})$$

is the Hartree-Fock interaction, and

$$F(t) = \frac{l^2}{\pi} \int d\mathbf{q} V_q^{HF} w_q(t) \quad (\text{B26})$$

describes the effects of the exciton-exciton correlations.

### APPENDIX C:

In this Appendix we derive the Pauli blocking contribution to the FWM signal in strong magnetic field, determined by Eq. (B4). Using Eq. (A6), the second term in Eq. (B4) satisfies

$$i\partial_t \mathcal{P}^\dagger(t) U \mathcal{P}^\dagger(t) |0\rangle = 2(\Omega_0 - i\Gamma) \mathcal{P}^\dagger(t) U \mathcal{P}^\dagger(t) |0\rangle + \mu \mathcal{E}_2(t) [U^\dagger U \mathcal{P}^\dagger(t) + \mathcal{P}^\dagger(t) U U^\dagger] |0\rangle \quad (\text{C1})$$

where we used the fact that  $\mathcal{P}^\dagger(t) |0\rangle$  is the zero-momentum exciton state with energy  $\Omega_0$ . Using the relation  $U^\dagger = N^{1/2} d_0^\dagger$  [see Eq. (5)] and noting that  $d_0^\dagger d_0 = 1$  when acting on the one-exciton state  $\mathcal{P}^\dagger(t) |0\rangle$ , while  $U U^\dagger |0\rangle = N d_0 d_0^\dagger |0\rangle = N |0\rangle$ , we obtain that

$$i\partial_t \mathcal{P}^\dagger(t) U \mathcal{P}^\dagger(t) |0\rangle = \Omega_0 \mathcal{P}^\dagger(t) U \mathcal{P}^\dagger(t) |0\rangle + 2N \mu \mathcal{E}_2(t) \mathcal{P}^\dagger(t) |0\rangle. \quad (\text{C2})$$

The non-interacting contribution to the two-exciton state,  $W_0^\dagger |0\rangle$ , is determined by Eq. (B1). After projecting with  $U$  on the lhs we obtain that

$$i\partial_t U W_0^\dagger(t) |0\rangle = 2\Omega_0 U W_0^\dagger(t) |0\rangle + \mu \mathcal{E}_2(t) U U^\dagger \mathcal{P}^\dagger(t) |0\rangle. \quad (\text{C3})$$

The last term can be simplified by using  $UU^\dagger\mathcal{P}^\dagger(t)|0\rangle = Nd_0d_0^\dagger\mathcal{P}^\dagger(t)|0\rangle = 2(N-1)\mathcal{P}^\dagger(t)|0\rangle$ , so that

$$i\partial_t UW_0^\dagger(t)|0\rangle = \Omega_0 UW_0^\dagger(t)|0\rangle + 2(N-1)\mu\mathcal{E}_p(t)\mathcal{P}^\dagger(t)|0\rangle. \quad (\text{C4})$$

Comparing the above equation to (C2), we see that  $UW_0^\dagger(t)|0\rangle = (1-1/N)\mathcal{P}^\dagger(t)U\mathcal{P}^\dagger(t)|0\rangle$ , and we thus obtain

$$U_{PB}^\dagger(t)|0\rangle = -\frac{1}{N}\mathcal{P}^\dagger(t)U\mathcal{P}^\dagger(t)|0\rangle. \quad (\text{C5})$$

Using the formal solution of Eq. (A6),

$$\mathcal{P}^\dagger(t) = -i\mu \int_{-\infty}^t dt' \mathcal{E}_2(t') e^{-iH(t-t')} U^\dagger e^{iH(t-t')}, \quad (\text{C6})$$

and that  $\mathcal{P}^\dagger(t)|0\rangle = p(t)U^\dagger|0\rangle$ , where the pump polarization  $p(t)$  is given by Eq. (24), we obtain

$$\phi_{PB}(t, t') = \frac{i\mu}{N} p(t') \int_{-\infty}^{t'} dt'' \mathcal{E}_2(t'') \langle 0|U e^{-iH(t-t')} e^{-iH(t'-t'')} U^\dagger e^{iH(t'-t'')} U U^\dagger|0\rangle. \quad (\text{C7})$$

Finally, using  $UU^\dagger|0\rangle = N|0\rangle$  and that  $U^\dagger|0\rangle$  is proportional to the magnetoexciton eigenstate of  $H$ , with eigenvalue  $\Omega_0$ , we obtain that

$$\phi_{PB}(t, t') = i\mu p(t') \int_{-\infty}^{t'} dt'' \mathcal{E}_2(t'') e^{-i\Omega_0(t-t'') - \Gamma|t-t''|}. \quad (\text{C8})$$

The Pauli blocking contribution to the FWM polarization is then calculated by substituting the above expression into Eq. (B6).

#### APPENDIX D:

In this Appendix we show the connection between our expression for the FWM signal, Eqs. (B6), (B7), and (B10), and that of Refs. 1,63,25. The equation for the four-wave-mixing polarization  $P_{XX}(t) = e^{i\omega_0 t} \tilde{P}_{XX}(t)$  can be obtained by taking the time derivative with respect to  $t$  of the rhs of Eq. (B6),

$$i\partial_t P_{XX}(t) = i\mu^2 \int_{-\infty}^t dt' \mathcal{E}_1^*(t') \left[ i\partial_t \phi_{XX}(t, t') - i\partial_t \phi_{XX}(t', t) \right]. \quad (\text{D1})$$

From Eq. (B10) we obtain after some algebra that

$$i\partial_t \phi_{XX}(t, t') = (\Omega_0 - i\Gamma) \phi_{XX}(t, t') \quad (\text{D2})$$

and

$$i\partial_t \phi_{XX}(t', t) = (\Omega_0 - i\Gamma) \phi_{XX}(t', t) + \left[ i\partial_t \chi(t) - 2\Omega_0 \chi(t) \right] e^{i\Omega_0(t-t') - \Gamma(t-t')}. \quad (\text{D3})$$

Substituting Eqs. (D2) and (D3) into Eq. (D1) and using Eq. (B24) we obtain a familiar equation for the FWM polarization:

$$i\partial_t P_{XX}(t) = (\Omega_0 - i\Gamma)P_{XX}(t) - \mu p_1^*(t) \left[ V^{HF} p^2(t) + F(t) \right], \quad (\text{D4})$$

where  $p_1(t)$  is the probe-induced polarization

$$p_1(t) = -i\mu \int_{-\infty}^t dt' e^{-i(\Omega_0 - i\Gamma)(t-t')} \mathcal{E}_1(t'). \quad (\text{D5})$$

The simple (momentum-independent) form of the above equation is due to the dispersionless energy spectrum of the electron and hole in the magnetic field. At zero field, a similar equation is obtained after averaging out over the spatial degrees of freedom.<sup>25,1,63</sup> The function  $F(t)$ , given by Eq. (B26), is determined by the two-exciton amplitude  $w_p(t)$ , satisfying Eq. (B14), and describes memory effects due to four-particle correlations. The APM<sup>12,70,25,1,63</sup> is recovered if one uses the simple model (47) for the memory function  $S(\omega)$ .

### APPENDIX E:

In this Appendix, we derive the long-time asymptotics of  $\chi(t)$ . For delta-function pump centered at  $t = 0$ , the pump polarization is simply  $p(t) = -i\mu \mathcal{E}_2 \theta(t) e^{-i\Omega_0 t - \Gamma t}$ , so that the Fourier transform of  $p^2(t)$  is

$$p^{(2)}(\omega) = \frac{-i(\mu \mathcal{E}_2)^2}{\omega - 2\Omega_0 + 2i\Gamma}. \quad (\text{E1})$$

Note that for short pump duration, we can write  $\chi(t) = e^{-i2\Omega_0 t} \tilde{\chi}(t)$ , where  $\tilde{\chi}(t)$  is the amplitude for zero detuning; therefore, it is sufficient to evaluate the Fourier transform of Eq. (35) at  $\Omega_0 = 0$ . For  $t \gg \Gamma^{-1}$ , the relevant frequencies are small,  $\omega \ll \Gamma$ , so that  $p^{(2)}(\omega) \simeq -(\mu \mathcal{E}_2)^2 / 2\Gamma$ , and  $\tilde{\chi}(t)$  takes the form

$$\tilde{\chi}(t) = -\frac{(\mu \mathcal{E}_2)^2}{4\pi\Gamma} V^{HF} \int_{-\infty}^{\infty} \frac{d\omega}{\omega} e^{-i\omega t} S(\omega). \quad (\text{E2})$$

In order to get  $\tilde{\chi}(t)$  for long times,  $t \gg D^{-1}$ , we substitute the low-frequency asymptotic expression (56) for the memory function (with  $\Omega_0 = 0$ ),

$$\tilde{\chi}(t) = -\frac{(\mu \mathcal{E}_2)^2}{4\pi\Gamma} V^{HF} [J_1(t) + J_2(t)], \quad (\text{E3})$$

where we separated out the contributions from the real and imaginary parts of  $S(\omega)$ :

$$J_1(t) = \int_{-\infty}^{\infty} \frac{d\omega}{\omega} \frac{e^{-i\omega t} \left( 1 + |G| \ln \left| \frac{2D}{\omega} \right| \right)}{\left( 1 + |G| \ln \left| \frac{2D}{\omega} \right| \right)^2 + \pi^2 |G|^2 \theta(\omega)} \quad (\text{E4})$$

$$J_2(t) = -i \int_0^{\infty} \frac{d\omega}{\omega} \frac{e^{-i\omega t} \pi |G|}{\left( 1 + |G| \ln \left| \frac{2D}{\omega} \right| \right)^2 + \pi^2 |G|^2 \theta(\omega)}. \quad (\text{E5})$$



Consider first  $J_1(t)$ . For  $t \gg D^{-1}$ , the characteristic frequencies are small, so that the second term in the denominator of the integrand can be neglected as compared to the logarithmic term. In this case, the main contribution comes from the imaginary part of the integrand,

$$J_1(t) \simeq -i \int_{-\infty}^{\infty} \frac{d\omega}{\omega} \frac{\sin \omega t}{1 + |G| \ln \left| \frac{2D}{\omega} \right|} \simeq \frac{-i\pi}{1 + |G| \ln 2Dt}. \quad (\text{E6})$$

Turning to  $J_2(t)$ , we notice that, for  $t \gg D^{-1}$ , the main contribution comes from the real part of the integrand. After omitting the second term in the denominator and integrating by parts, we obtain

$$J_2(t) \simeq -i\pi t \int_0^{\infty} \frac{d\omega \sin \omega t}{1 + |G| \ln \left| \frac{2D}{\omega} \right|} \simeq \frac{-i\pi}{1 + |G| \ln 2Dt}. \quad (\text{E7})$$

One can show that the subleading terms are  $\sim |G| \left(1 + |G| \ln 2Dt\right)^{-2}$ . Note that the imaginary and real parts of  $S(\omega)$  contribute *equally* to the long-time asymptotics. Finally, substituting Eqs. (E6) and (E7) into Eq. (E3), we arrive at Eq. (57).

## REFERENCES

- <sup>1</sup> For a recent review see D. S. Chemla, in *Nonlinear Optics in Semiconductors*, edited by R. K. Willardson and A. C. Beers (Academic Press, 1999).
- <sup>2</sup> See, e.g., H. Haug and S. W. Koch, *Quantum theory of the optical and electronic properties of semiconductors*, 2nd edition (World Scientific, Singapore, 1993).
- <sup>3</sup> See, e.g., S. Mukamel, *Principles of Nonlinear Optical Spectroscopy*, (Oxford University Press, 1995).
- <sup>4</sup> See, e.g., J. Shah, *Ultrafast Spectroscopy of Semiconductors and Semiconductor Nanostructures* (Springer, New York, 1996).
- <sup>5</sup> T. Yajima and Y. Taira, J. Phys. Soc. Jpn. **47**, 1620 (1979).
- <sup>6</sup> S. Schmitt-Rink, and D. S. Chemla, Phys. Rev. Lett. **57**, 2752 (1986).
- <sup>7</sup> S. Schmitt-Rink, D. S. Chemla, and H. Haug, Phys. Rev. B **37**, 941 (1988).
- <sup>8</sup> M. Lindberg and S. W. Koch, Phys. Rev. B **38**, 3342 (1988).
- <sup>9</sup> M. Lindberg and S. W. Koch, Phys. Rev. B **40**, 4095 (1989).
- <sup>10</sup> R. Binder, S. W. Koch, M. Lindberg, W. Schäfer, and F. Jahnke, Phys. Rev. B **43**, 6520 (1991).
- <sup>11</sup> K. Leo, M. Wegener, J. Shah, D. S. Chemla, I. O. Göbel, T. C. Damen, S. Schmitt-Rink, and W. Schäfer, Phys. Rev. Lett. **65**, 1340 (1990).
- <sup>12</sup> M. Wegener, S. Schmitt-Rink, D. S. Chemla, and W. Schäfer, Phys. Rev. A **42**, 5675 (1990).
- <sup>13</sup> S. Weiss, M.-A. Mycek, S. Schmitt-Rink, and D. S. Chemla, Phys. Rev. Lett. **69**, 2685 (1992).
- <sup>14</sup> M. Lindberg, R. Binder, and S. W. Koch, Phys. Rev. A **45**, 1865 (1992).
- <sup>15</sup> S. Glutsch, U. Siegner, and D. S. Chemla, Phys. Rev. B **52**, 4941 (1995).
- <sup>16</sup> J.-Y. Bigot, M.-A. Mycek, S. Weiss, R. G. Ulbrich, and D. S. Chemla, Phys. Rev. Lett. **70**, 3307 (1993).
- <sup>17</sup> D. S. Chemla, J.-Y. Bigot, M.-A. Mycek, S. Weiss, and W. Schäfer, Phys. Rev. B **50**, 8439 (1994).
- <sup>18</sup> See, e.g., V. M. Axt and S. Mukamel, Rev. Mod. Phys. **70**, 145 (1998).
- <sup>19</sup> H. Wang, K. B. Ferrio, D. G. Steel, Y. Z. Hu, R. Binder, and S. W. Koch, Phys. Rev. Lett. **71**, 1261 (1993).
- <sup>20</sup> H. Wang, K. B. Ferrio, D. G. Steel, P. R. Berman, Y. Z. Hu, R. Binder, and S. W. Koch, Phys. Rev. A **49**, 1551 (1994).
- <sup>21</sup> Y. Z. Hu, R. Binder, S. W. Koch, S. T. Cundiff, H. Wang, and D. G. Steel, Phys. Rev. B **49**, 14 382 (1994).
- <sup>22</sup> T. Rappen, U. G. Peter, M. Wegener, and W. Schäfer, Phys. Rev. B **49**, 10 774 (1994).
- <sup>23</sup> M. Lindberg, Y. Z. Hu, R. Binder, and S. W. Koch, Phys. Rev. B **50**, 18 060 (1994).
- <sup>24</sup> V. M. Axt, A. Stahl, E. J. Mayer, P. H. Bolivar, S. Nüsse, K. Ploog, and K. Köhler, Phys. Status Solidi B **188**, 447 (1995).
- <sup>25</sup> W. Schäfer, D. S. Kim, J. Shah, T. C. Damen, J. E. Cunningham, K. W. Goossen, L. N. Pfeiffer, and K. Köhler, Phys. Rev. B **53**, 16 429 (1996).
- <sup>26</sup> B. F. Feuerbacher, J. Kuhl, and K. Ploog, Phys. Rev. B **43**, 2439 (1991).
- <sup>27</sup> S. Bar-Ad and I. Bar-Joseph, Phys. Rev. Lett. **68**, 349 (1992).
- <sup>28</sup> D. J. Lovering, R. T. Phillips, G. J. Denton, and G. W. Smith, Phys. Rev. Lett. **68**, 1880 (1992).

- <sup>29</sup> K.-H. Pantke, D. Oberhauser, V. G. Lyssenko, J. M. Hvam, and G. Weimann, *Phys. Rev. B* **47**, 2413 (1993).
- <sup>30</sup> K. Bott, O. Heller, D. Bennhardt, S. T. Cundiff, P. Thomas, E. J. Mayer, G. O. Smith, R. Eccleston, J. Kuhl, and K. Ploog, *Phys. Rev. B* **48**, 17 418 (1993).
- <sup>31</sup> E. J. Mayer, G. O. Smith, V. Heuckeroth, J. Kuhl, K. Bott, A. Schulze, T. Meier, D. Bennhardt, S. W. Koch, P. Thomas, R. Hey, and K. Ploog, *Phys. Rev. B* **50**, 14 730 (1994).
- <sup>32</sup> E. J. Mayer, G. O. Smith, V. Heuckeroth, J. Kuhl, K. Bott, A. Schulze, T. Meier, S. W. Koch, P. Thomas, R. Hey, and K. Ploog, *Phys. Rev. B* **51**, 10 909 (1995).
- <sup>33</sup> C. Sieh, T. Meier, F. Jahnke, A. Knorr, S. W. Koch, P. Brick, M. Hübner, C. Ell, J. Prineas, G. Khitrova, and H. M. Gibbs, *Phys. Rev. Lett.* **82**, 3112 (1999).
- <sup>34</sup> T. Aoki, G. Mohs, M. Kuwata-Gonokami, and A. A. Yamaguchi, *Phys. Rev. Lett.* **82**, 3108 (1999).
- <sup>35</sup> F. C. Spano and S. Mukamel, *Phys. Rev. Lett.* **66**, 1197 (1991).
- <sup>36</sup> J. A. Leegwater and S. Mukamel, *Phys. Rev. A* **46**, 452 (1992).
- <sup>37</sup> V. Chernyak and S. Mukamel, *Phys. Rev. B* **48**, 2953 (1993).
- <sup>38</sup> I. Balslev and E. Hanamura, *Solid State Comm.* **72**, 843 (1989).
- <sup>39</sup> V. M. Axt and A. Stahl, *Z. Phys. B* **93**, 195 (1994).
- <sup>40</sup> K. Victor, V. M. Axt, and A. Stahl, *Phys. Rev. B* **51**, 14 164 (1995).
- <sup>41</sup> V. M. Axt, G. Bartels, and A. Stahl, *Phys. Rev. Lett.* **76**, 2543 (1996).
- <sup>42</sup> Th. Östreich, K. Schönhammer, and L. J. Sham, *Phys. Rev. Lett.* **74**, 4698 (1995).
- <sup>43</sup> Th. Östreich, K. Schönhammer, and L. J. Sham, *Phys. Rev. B* **58**, 12920 (1998).
- <sup>44</sup> Th. Östreich and L. J. Sham, *Phys. Rev. Lett.* **83**, 3510 (1999).
- <sup>45</sup> I. E. Perakis and D. S. Chemla, *Phys. Rev. Lett.* **72**, 3202 (1994).
- <sup>46</sup> I. E. Perakis and T. V. Shahbazyan, *Int. J. Mod. Phys. B* **13**, 869 (1999).
- <sup>47</sup> N. Primožich, T. V. Shahbazyan, I. E. Perakis, and D. S. Chemla, *Phys. Rev. B* **61**, 2041 (2000).
- <sup>48</sup> T. V. Shahbazyan, N. Primožich, I. E. Perakis, and D. S. Chemla, *Phys. Rev. Lett.* **84**, 2006 (2000).
- <sup>49</sup> I. E. Perakis and T. V. Shahbazyan, to appear in *Surf. Sci. Reports*.
- <sup>50</sup> I. E. Perakis, I. Brener, W. H. Knox, and D. S. Chemla, *J. Opt. Soc. Am. B* **13**, 1313 (1996).
- <sup>51</sup> I. E. Perakis, *Chem. Phys.* **210**, 259 (1996).
- <sup>52</sup> C. Stafford, S. Schmitt-Rink, and W. Schaefer, *Phys. Rev. B* **41**, 10 000 (1990).
- <sup>53</sup> S. Glutsch and D. S. Chemla *Phys. Rev. B* **52**, 8317 (1995).
- <sup>54</sup> J. B. Stark, W. H. Knox, D. S. Chemla, W. Schaefer, S. Schmitt-Rink, and C. Stafford, *Phys. Rev. Lett* **65**, 3033 (1990).
- <sup>55</sup> O. Carmel and I. Bar-Joseph, *Phys. Rev. B* **47**, 7606 (1993).
- <sup>56</sup> T. Rappen, J. Schröder, A. Leisse, M. Wegener, W. Schäfer, N. J. Sauer, and T. Y. Chang, *Phys. Rev. B* **44**, 13 093 (1991).
- <sup>57</sup> S. T. Cundiff, M. Koch, W. H. Knox, and J. Shah, *Phys. Rev. Lett.* **77**, 1107 (1996).
- <sup>58</sup> M. Jiang, H. Wong, R. Merlin, D. G. Steel, and M. Cardona, *Phys. Rev. B* **48**, 15 476 (1993).
- <sup>59</sup> U. Siegner, M.-A. Mycek, S. Glutch, and D. S. Chemla, *Phys. Rev. Lett.* **74**, 470 (1995).
- <sup>60</sup> U. Siegner, M.-A. Mycek, S. Glutch, and D. S. Chemla, *Phys. Rev. B* **51**, 4953 (1995).

- <sup>61</sup> P. Kner, S. Bar-Ad, M.V. Marquezini, D.S. Chemla and W. Schäfer, Phys. Rev. Lett. **78**, 1319 (1997).
- <sup>62</sup> P. Kner, W. Schäfer, R. Lövenich, and D. S. Chemla, Phys. Rev. Lett. **81**, 5386 (1998).
- <sup>63</sup> P. Kner, S. Bar-Ad, M.V. Marquezini, D.S. Chemla, R. Lövenich and W. Schäfer, Phys. Rev. B **60**, 4731 (1999).
- <sup>64</sup> V. Chernyak, S. Yokojima, T. Meier, and S. Mukamel, Phys. Rev. B **58**, 4496 (1998).
- <sup>65</sup> S. Yokojima, T. Meier, V. Chernyak, and S. Mukamel, Phys. Rev. B **59**, 12 584 (1999).
- <sup>66</sup> I. V. Lerner and Yu. E. Lozovik, Zh. Exp. Teor. Fiz. **80**, 1488 (1981) [Sov. Phys.-JETP **53**, 763 (1981)].
- <sup>67</sup> Yu. A. Bychkov, E. I. Rashba Zh. Exp. Teor. Fiz. **85**, 1826 (1983) [Sov. Phys.-JETP **58**, 1062 (1983)].
- <sup>68</sup> D. Paquet, T. M. Rice, and K. Ueda, Phys. Rev. B **32**, 5208 (1985).
- <sup>69</sup> N. A. Fromer, C. Schüller, D. S. Chemla, T. V. Shahbazyan, I. E. Perakis, K. Maranowski and A. C. Gossard, Phys. Rev. Lett. **83**, 4646 (1999).
- <sup>70</sup> S. Schmitt-Rink, S. Mukamel, K. Leo, J. Shah, and D. S. Chemla, Phys. Rev. A **44**, 2124 (1991).
- <sup>71</sup> H. Zhou, A. V. Nurmikko, C.-C. Chu, H. Han, R. L. Gunshor, and T. Takagahara, Phys. Rev. B **58**, R10131 (1998).

## FIGURES

FIG. 1. The memory function  $S(\omega)$  for attractive exciton-exciton interaction calculated from Eq. (36) with  $a/l = 3.0$  and  $u_0/E_0 = 0.05$  (solid line),  $u_0/E_0 = 0.4$  (dotted line), and  $u_0/E_0 = 0.8$  (dashed line). The oscillator strength of the biexciton resonance increases with  $u_0$ .

FIG. 2. The memory function  $S(\omega)$  for attractive exciton-exciton interaction with  $a/l = 3.0$  and  $u_0/E_0 = -0.05$  (solid line),  $u_0/E_0 = -0.4$  (dotted line), and  $u_0/E_0 = -0.8$  (dashed line). With increasing  $|u_0|$ , the asymmetric band of exciton-exciton scattering states transforms into a narrow antibound resonance.

FIG. 3. Calculated TI-FWM signal for short pump duration,  $t_0E_0 = 0.5$ , for  $a/l = 6.0$ ,  $\Gamma/E_0 = 0.0125$ ,  $\gamma_b/E_0 = 0.005$ ,  $\Omega_0 = 0$ , with  $u_0/E_0 = 0.05$  (solid curve) and  $u_0/E_0 = 0.4$  (dashed curve). The period of the biexciton oscillations is  $T_b = 2\pi/E_b \simeq 2\pi/u_0$ .

FIG. 4. Calculated SR-FWM signal for  $u_0/E_0 = 0.4$ , and the rest of the parameters same as in Fig. 3. The exciton peak strength oscillates with the biexciton period  $T_b = 2\pi/E_b \simeq 2\pi/u_0$ .

FIG. 5. Calculated TI-FWM signal at intermediate magnetic field,  $a/l = 3.0$ , for  $u_0/E_0 = 0.05$  (solid line),  $u_0/E_0 = 0.4$  (dotted line), and  $u_0/E_0 = 0.8$  (dashed line) with (a) short pump duration,  $t_0E_0 = 0.5$ , and (b) long pump duration,  $t_0E_0 = 5.0$ . The rest of parameters same as in Fig. 3.

FIG. 6. Calculated SR-FWM signal for  $u_0 = 0.4$ , pump tuned to exciton,  $\Omega_0 = 0$ , and long pulse duration,  $t_0E_0 = 5.0$ . The biexciton peak is suppressed while the exciton peak decays with characteristic time  $(2\Gamma)^{-1}$  for  $\tau > 0$ . The rest of parameters same as in Fig. 5.

FIG. 7. Calculated SR-FWM signal for the pump tuned to biexciton,  $2\Omega_0 = E_b$ . For  $\tau > 0$ , biexciton peak decays with characteristic time  $(2\Gamma)^{-1}$  while exciton peak follows the pump. The rest of parameters same as in Fig. 6.

FIG. 8. Comparison of TI-FWM signals calculated using the analytical solution (34-36) (dotted curve) and the APM (47) (dashed curve) with the exact numerical calculations (solid curve) for  $a/l = 1.5$ ,  $u_0/|E_0| = 0.4$  with (a)  $\gamma_b = 0.005E_0$  and (b)  $\gamma_b = 2\Gamma = 0.025E_0$ . The rest of parameters same as in Fig. 3.

FIG. 9. Calculated TI-FWM signal for repulsive interaction with  $G = -6.0$  (solid line),  $G = -4.8$  (dotted line),  $G = -3.6$  (dashed line),  $G = -1.2$  (long-dashed line), and  $G = -0.24$  (dot-dashed line), with (a)  $\Gamma/E_0 = 0.0125$  and (b)  $\Gamma/E_0 = 0.05$ . For larger  $|G|$ , the decay is exponential with the interaction-induced characteristic time  $\gamma_{sc}^{-1}$ . For smaller  $|G|$ , the exponential decay is followed by the nonexponential tail for large  $|\tau|$ . The rest of the parameters are the same as in Fig. 3.

FIG. 10. (a) Comparison of TI-FWM signals calculated using analytical solution (34-36) (dotted curve) and the APM (48) (dashed curve) with the exact numerical calculations (solid curve) for  $a/l = 3.0$ ,  $G = -1.2$  with  $\Gamma/E_0$  and  $t_0E_0 = 0.5$ . The exponential decay at initial time delays is followed by the power law decay for large  $|\tau|$ . (b) Real (upper curve) and imaginary (lower curve) parts of the memory function fitted by a Lorentzian (dotted line). The Lorentzian width determines the exponential decay of the signal in the APM. The deviation of  $S(\omega)$  from the Lorentzian at low frequencies leads to the power-law decay for large  $|\tau|$ .

FIG. 11. Same as Fig. 10, but for weaker magnetic field,  $a/l = 1.5$ . The crossover to the nonexponential regime occurs at earlier time delays.

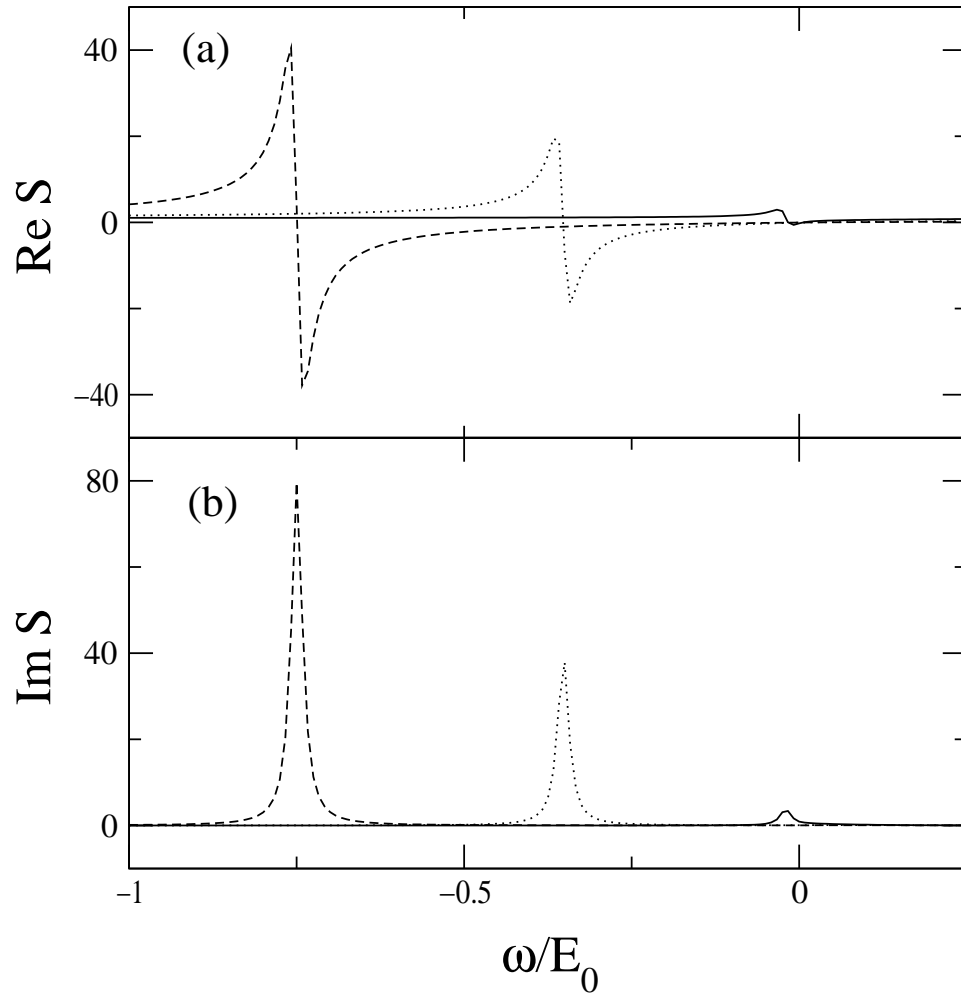


Fig. 1

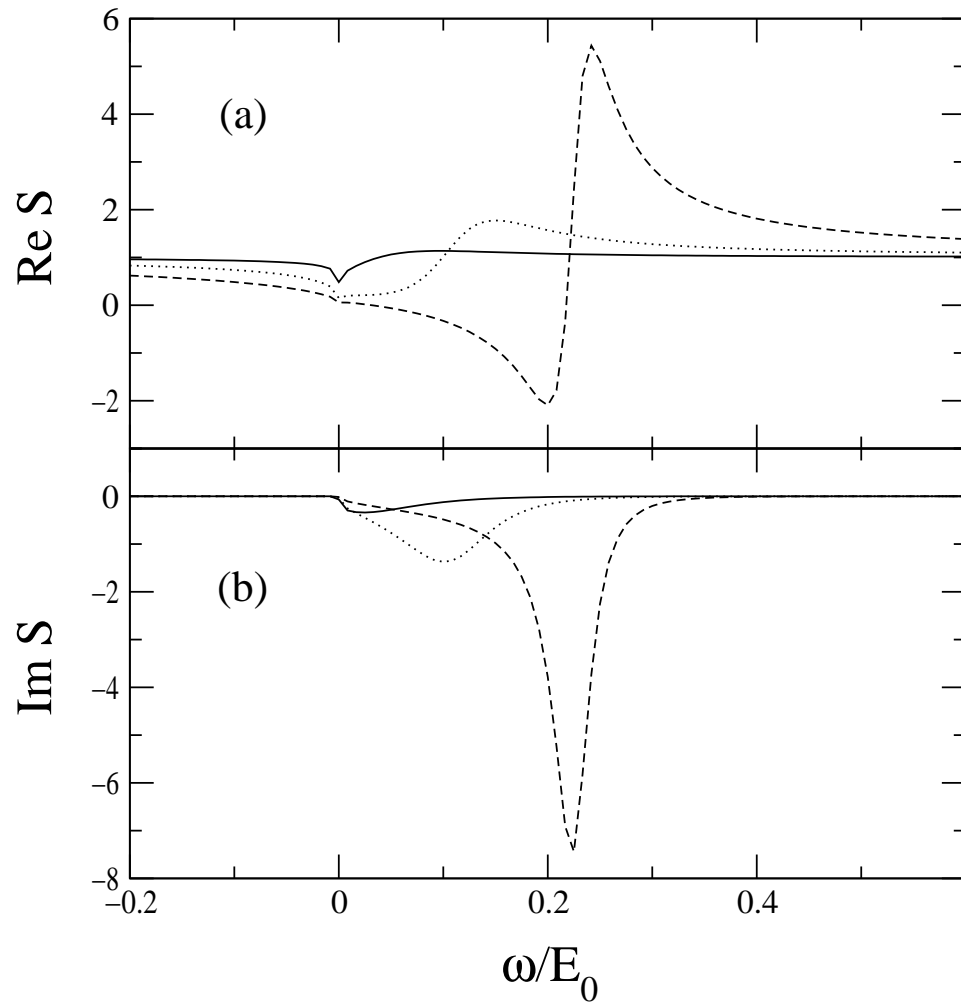


Fig. 2



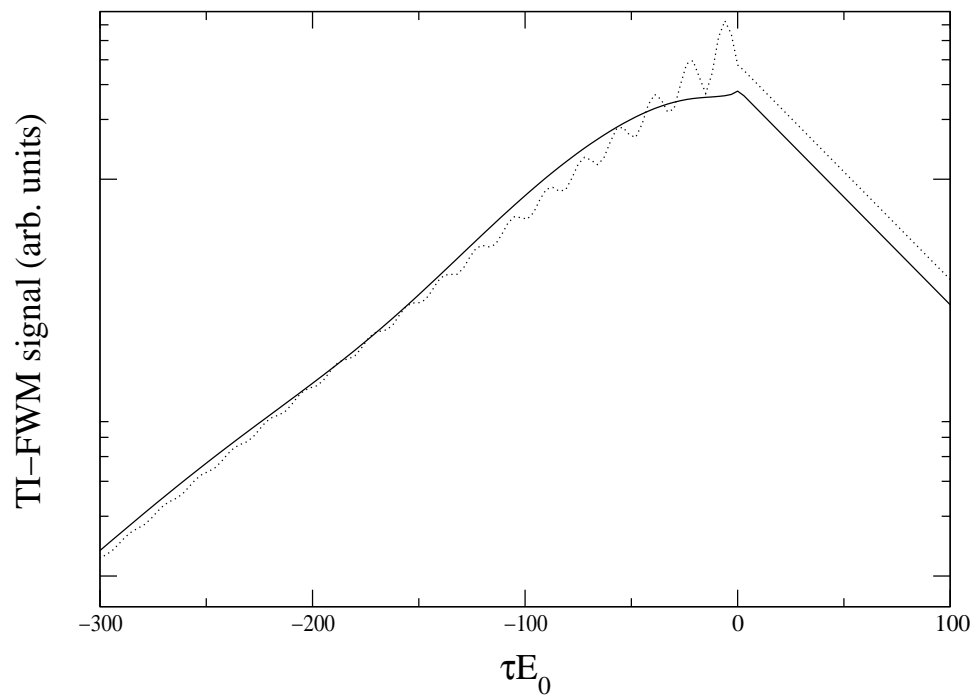


Fig. 3

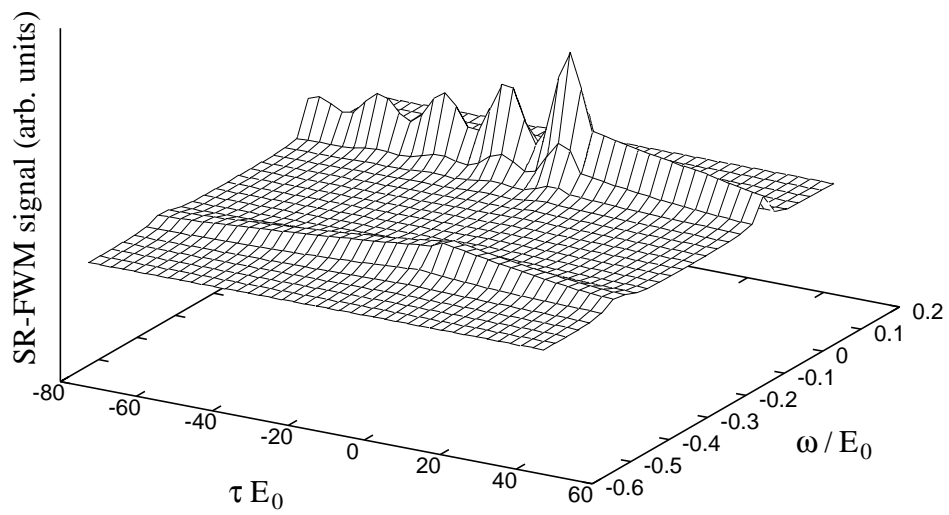


Fig. 4

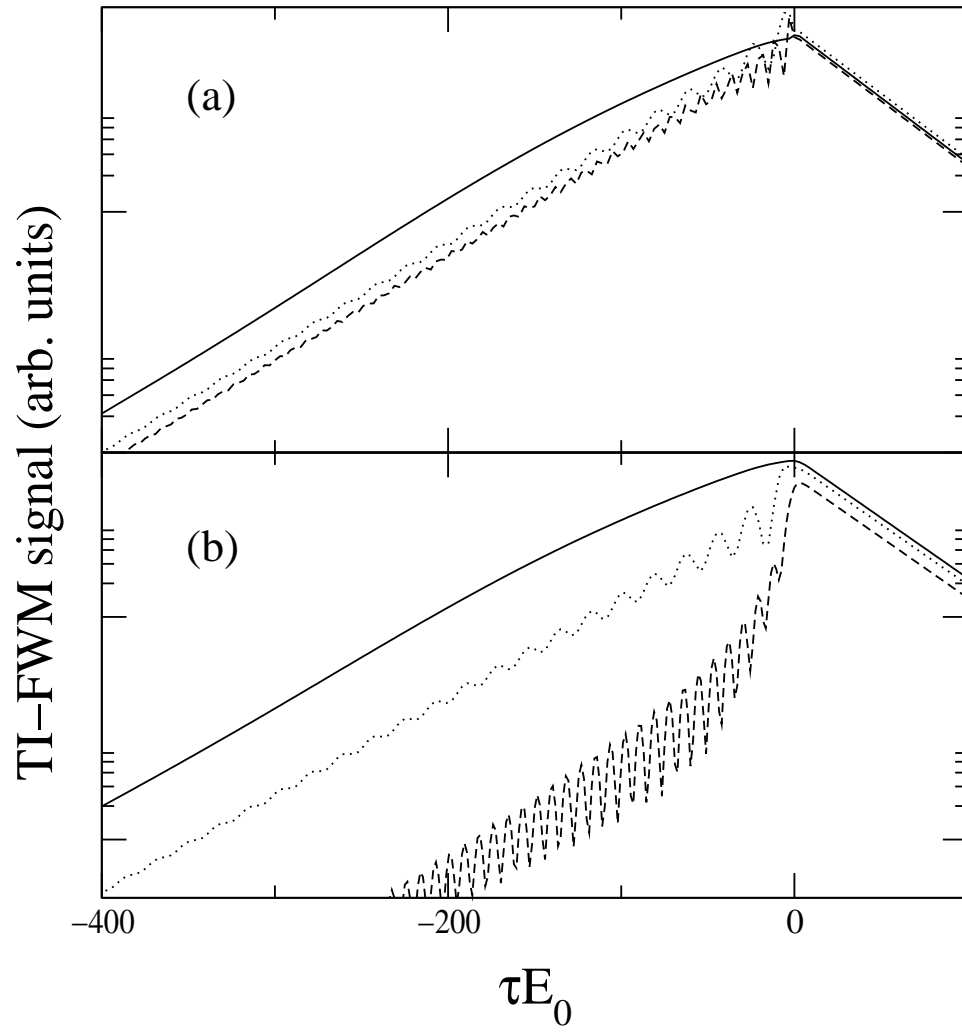


Fig. 5

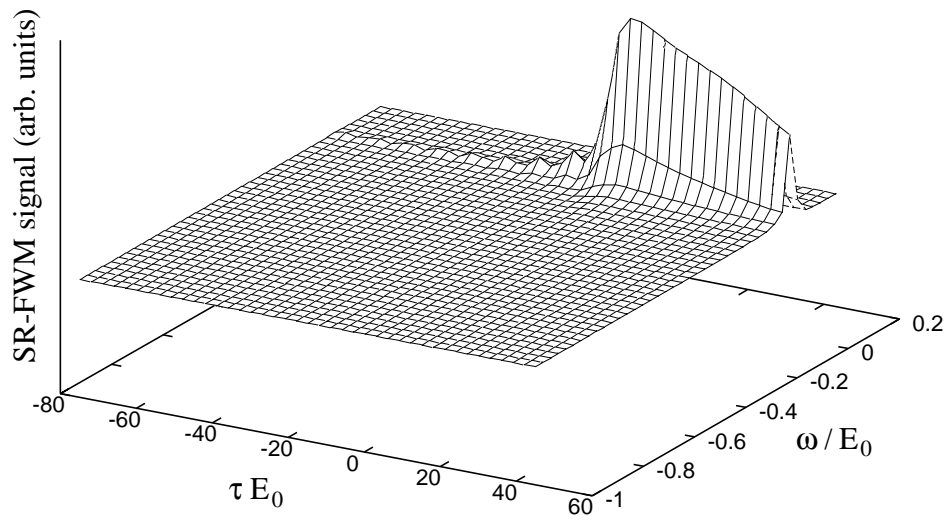


Fig. 6

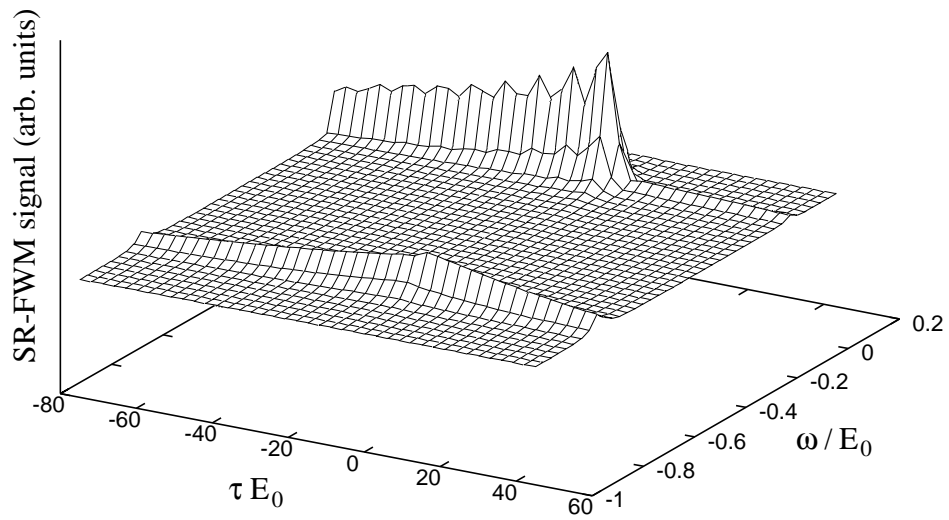


Fig. 7

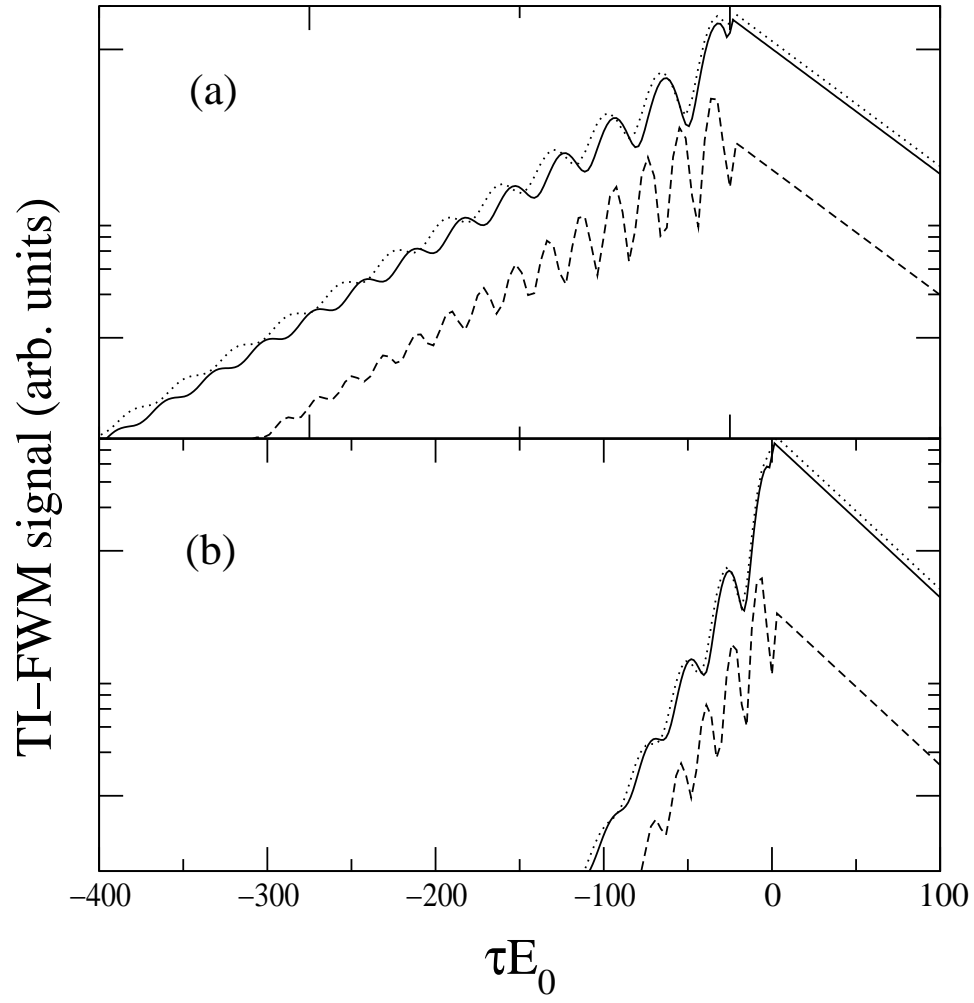


Fig. 8

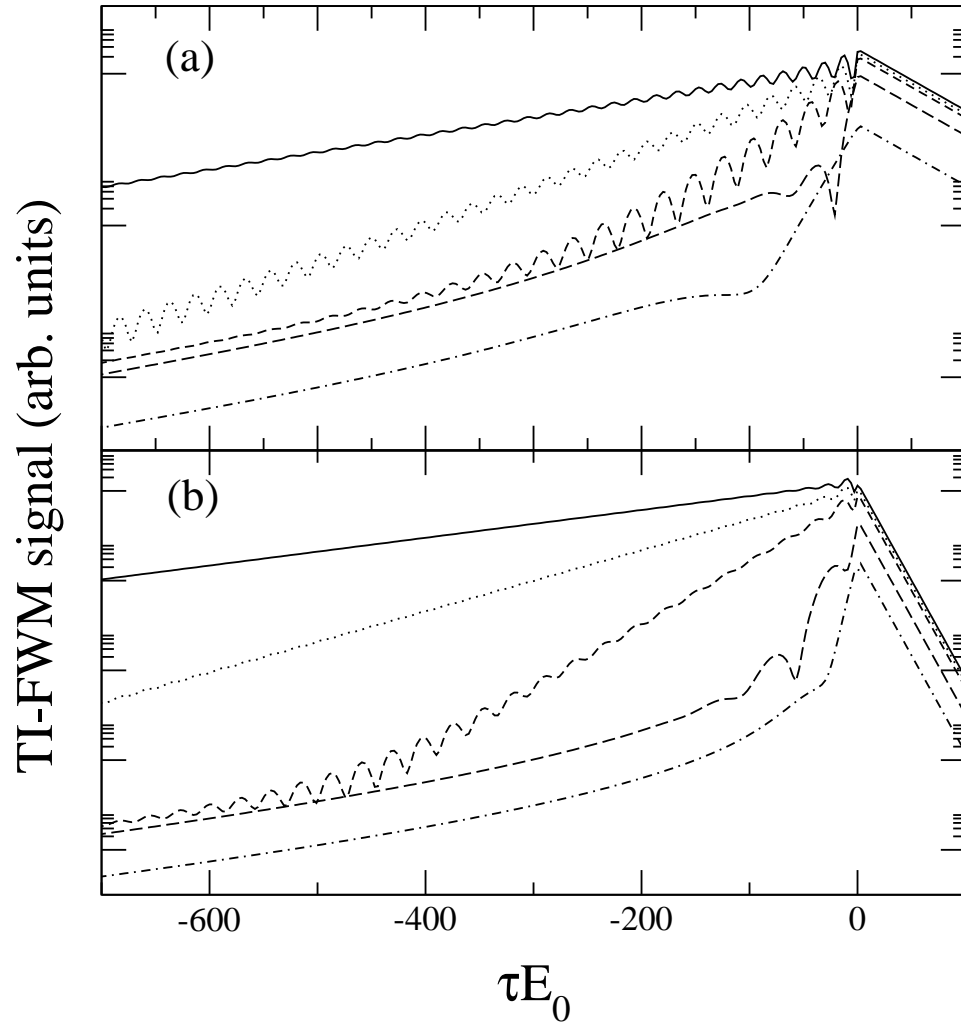


Fig. 9

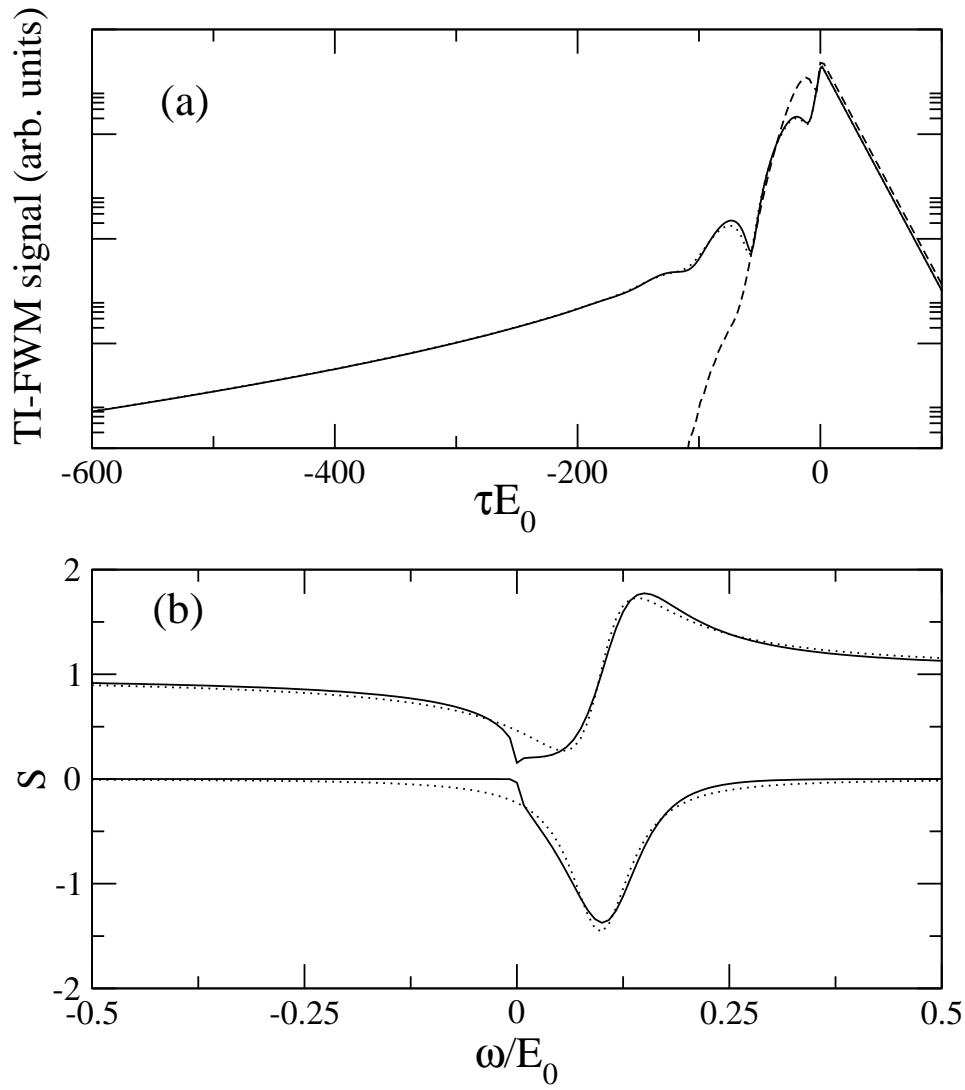


Fig. 10



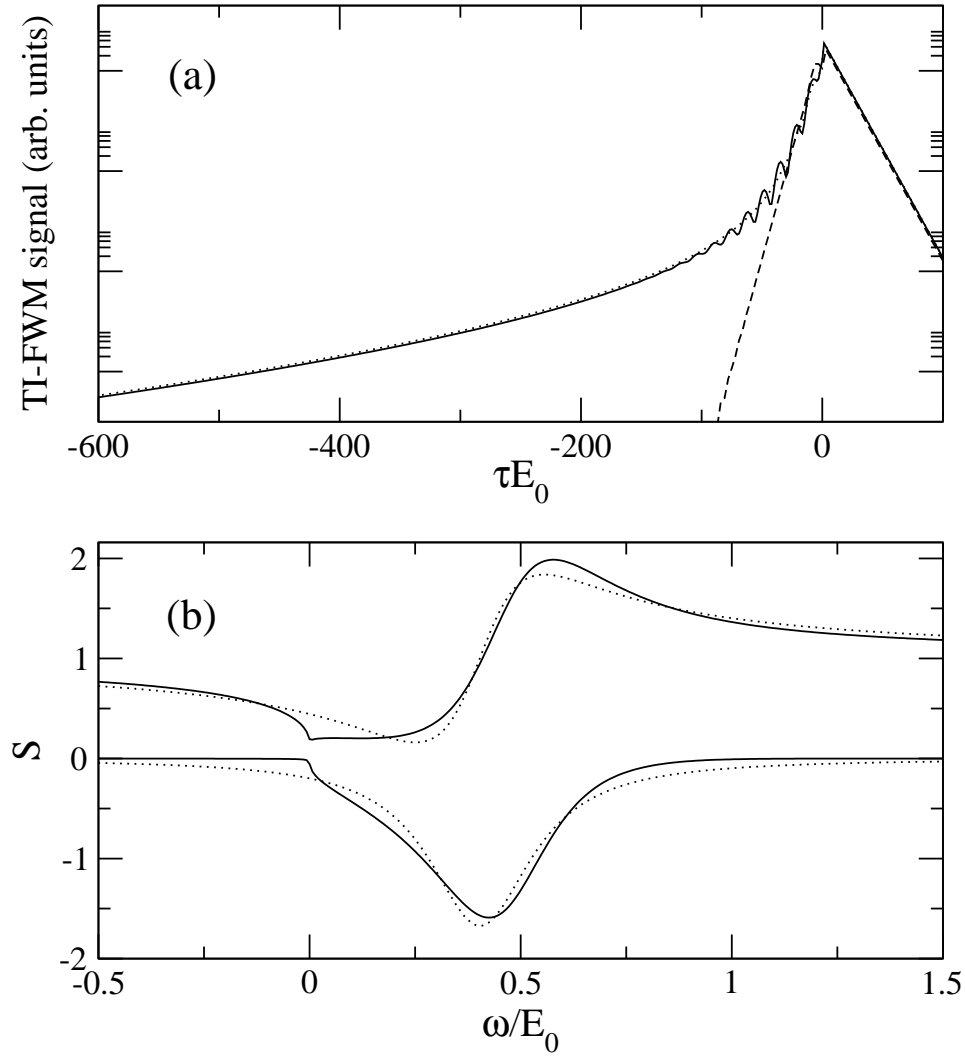


Fig. 11